KTH Electrical Engineering

Electromagnetic Modelling of Power Transformers with DC Magnetization

Seyed Ali Mousavi

Licentiate Thesis in Electromagnetic Engineering

Stockholm, Sweden 2012

Royal Institute of Technology (KTH)
School of Electrical Engineering
Division of Electromagnetic Engineering
Teknikringen 33
SE– 100 44 Stockholm, Sweden

TRITA-EE 2012:057
ISSN 1653-5146
ISBN 978-91-7501-537-8

Akademisk avhandling som med tillstånd av Kungliga Tekniska Högskolan framläggs till offentlig granskning för avläggande av teknologie licentiatexamen torsdagen den 29 november 2012 klockan 10.00 i sal F3, Lindstedtsvägen 26, Kungliga Tekniska Högskolan, Stockholm.

© Seyed Ali Mousavi, November 2012
Tryck: Universitetsservice US AB

To my Parents

Abstract

DC currents that flow through the ground can be injected to the star windings of power transformers from their grounded neutral points and close their path with transmission lines. The geomagnetically induced currents (GICs) and AC/DC convertors of high voltage direct current (HVDC) systems are the sources of such DC currents. These currents may cause saturation of the core in power transformers that leads to destruction in the transformer performance. This phenomenon results in unwanted influences on power transformers and the power system. Very asymmetric magnetization current, increasing losses and creation of hot spots in the core, in the windings, and the metallic structural parts are adverse effects that occur in transformers. Also, increasing demand of reactive power and misoperation of protective relays menaces the power network. Damages in large power transformers and blackouts in networks have occurred due to this phenomenon.

Hence, studies regarding this subject have taken the attention of researchers during the last decades. However, a gap of a comprehensive analysis still remains. Thus, the main aim of this project is to reach to a deep understanding of the phenomena and to come up with a solution for a decrease of the undesired effects of GIC.

Achieving this goal requires an improvement of the electromagnetic models of transformers which include a hysteresis model, numerical techniques, and transient analysis.

In this project until now, a new algorithm for digital measurement of the core materials is developed and implemented. It enhances the abilities of accurate measurements and an improved hysteresis model has been worked out. Also, a novel differential scalar hysteresis model is suggested that easily can be implemented in numerical methods. Three dimensional finite element models of various core types of power transformers are created to study the effect on them due to DC magnetization. In order to enhance the numerical tools for analysis of low frequency transients related to power transformers and the network, a distributed reluctance network method has been outlined. In this thesis a method for solving such a network problem with coupling to an electrical circuit and taking hysteresis into account is suggested.

Index terms: Transformer, Hysteresis, DC magnetization, GICs, FEM, reluctance network method.

Acknowledgements

This Licentiate thesis is based on results within the research group of Electrotechnical Modeling, at the Department of Electromagnetic Engineering, School of Electrical Engineering, Royal Institute of Technology (KTH).
First and foremost, I would like to thank my supervisor Professor Göran Engdahl for his valuable guidance and advice, and for inspiring me and motivating me in this project. Göran, you were not only my supervisor, you were more my teacher. I learned a lot from you as one of nicest men that I have known.
This research project would not have been possible without the support of many people. I wish to express my sincere gratitude to my friend, good man and great engineer Andreas Krings, without whose collaboration I could not have completed the main part of the project.
I would like to gratefully acknowledge my reference group and the people from ABB who gave me the industrial insight and enlightened my way in this work: Dr. Dierk Bormann, Dr. Mikael Dahlgren, Dr. Kurt Gramm and Dr. Torbjorn Wass and the other reference group members.
I would like to thank the former PhD students in our group from whose great recommendations and guidance I benefitted: Dr. David Ribbenfjärd, Dr. Nathaniel Taylor and Dr. Hanif Tavakoli.
I am also thankful to Peter Lönn for his technical support with computer hardware and software and Carin Norberg for her kind help with administration support.
I'm sincerely grateful to my dear buddies for their friendship, kind help and the many things I have learned from them: Mohamad, Alireza, Shafig, Nadija, Ara, Xiaolei, Respicius, Jesper, Johanna, Erfan, Shahab, Afshin, Amin, Ebrahim, Angela, Claes and all my other colleagues in the EE school.
I also thank Professor Rajeev Thottappillil, Head of the Department, for trusting me enough to employ me and create a friendly environment for my research work.
Last but not least, my deepest gratitude goes to my family for their unflagging love and support throughout my life; this dissertation would have been simply impossible without them. I am indebted to my father, mother and sister for their care and love.

Ali Mousavi
Stockholm, Sweden,
October 2012.

List of Publications

Appended Papers

Paper I. **S. A. Mousavi**, and G. Engdahl, "Differential Approach of Scalar Hysteresis Modeling based on the Preisach Theory ", IEEE Transaction of Magnetic, VOL 47, No. 10, pp. 3040-3043, Oct 2011.

Paper II. **S. A. Mousavi**, and G. Engdahl, Edris Agheb, "Investigation of GIC Effects on Core Losses in Single Phase Power Transformers", journal of ARCHIVES OF ELECTRICAL ENGINEERING, Vol. 60(1), pp. 35-47, 2011.

Paper III. **S. A. Mousavi,** and G. Engdahl, "Implementation of Hysteresis Model in Transient Analysis of Nonlinear Reluctance Networks", ICEMS 2012, Oct 2012, Sapporo, Japan.

Paper IV. **S. A. Mousavi**, G. Engdahl, M. Mohammadi, and V. Nabaei, "Novel Method for Calculation of Losses in Foil Winding Transformers under Linear and non-Linear loads by Using Finite Element Method", Advanced Research Workshop on Transformers ARWtr2010, 3-6 October 2010, Santiago de Compostela, Spain, ISBN: 978-84-614-3528-9.

Additional publications not appended

Paper V. E. Agheb, E. Hashemi, **S. A. Mousavi**, and H. K. Hoidalen, "Study of Very Fast Transient Over voltages in Air-cored Pulsed Transformers", COMPEL, Vol. 31, No. 2, 2012, pp. 658-669.

Paper VI. **S. A. Mousavi,** and G. Engdahl "Three dimensional finite element analyses of transformer core joints with respect to the magnetization current", MMM 56th, Arizona, 30 Oct - 3Nov, 2011.

Paper VII. **S. A. Mousavi**, and Göran Engdahl, "Differential Approach of Scalar Hysteresis Modeling based on the Preisach Theory ", Intermag 2011, Taipei, Taiwan, 25-29 April.

Paper VIII. **S. A. Mousavi**, G. Engdahl, and E. Agheb, "Investigation of GIC Effects on Core Losses in Single Phase Power Transformers", XXI symposium Electromagnetic Phenomena in Nonlinear Circuits EPNC2010, June 29-July 2, 2010, Dortmund and Essen, Germany, ISBN: 978-83-921340-8-4.

Paper IX. A.Krings, **S. A. Mousavi**, O. Wallmark, and J. soulard, "Thermal Influence on the Magnetic Properties and Iron Losses in", accepted to oral presentation in 12th joint MMM/Intermag Conference, 14–18 January 2013, Chicago, Illinois, USA.

Author's contributions in the listed papers

In the papers that the author of this thesis is the first author, the main idea and the body of the papers belong to him. The co-authors have contributed in the revise of the papers and have supplied the required data, material, and measurements. For the other papers the author of this thesis has contributed partly in the related projects.

Contents

Chapter1

1 Background

1.1 Introduction

The existence of superimposed DC currents in power networks may saturate power transformers and cause considerable adverse effects on power transformers and power networks [1] [2] [3]. The main source of DC currents is geomagnetically induced currents (GICs) which can be created by interaction between solar wind and the Earth's magnetic field [4]. The frequencies of these currents are very low and they are quasi-DC [1]. Countries close to the earth's poles such as Sweden, Norway, Canada and Russia are more vulnerable to GICs. Also, using High Voltage DC transmission (HVDC), which is growing in the world, can create a source of DC magnetization for power transformers in the network [5] [6].
DC currents can be injected in three-phase transformers or banks of single-phase transformers with a neutral point of grounded star-connected windings, and cause the transformer core to be saturated during one of the half cycles of each supply voltage period [1]. It is notable that a small DC current, due to the number of winding turns, can create a huge MMF inside the core. This phenomenon has several adverse effects on the performance of power transformers, such as increasing core and winding losses, stray losses in tank and metallic constructions and noise levels [1] [7] [8].
The duration of GICs can be in the order of several minutes to several hours. The value of the DC current can reach 100A [1]. Consequently, permanent damage or at least reduced lifetime due to overheating can occur in power transformers [9]. From the viewpoint of the power grid, the existence of GICs primarily involves a risk of voltage collapse due to imbalances in the need for reactive compensation, resulting in serious voltage drops [10]. Also, DC magnetization causes the creation of odd and even harmonics in the power system [11] [12]. These harmonics cause an increase of the stray losses inside

the transformers and also incorrect tripping of relays in power generators and capacitive filter banks [13].
Several researches have performed investigations of this phenomenon and its effects on power transformers and power networks [1]- [14]. However, a comprehensive study where appropriate models of transformers are used, is considered to be missing.

1.2 Aims of the project

The main aim of this project is to develop a comprehensive electromagnetic model of power transformers in order to investigate the influence of DC magnetization on power transformers and the power network. To achieve this goal it is necessary to perform several tasks in the field of material modeling, measurement, transformer modeling and studying the interaction of transformer and power networks. The first half of this project has been devoted to this Licentiate thesis. It will be continued in form of a PhD project.
A superimposed DC current causes an asymmetric magnetization of the transformer core. This means that the material traverses a minor asymmetric magnetic hysteresis loops. From the modeling point of view, this is a challenge, because a proper hysteresis model is required to predict the resulting asymmetric loops. Measurements of magnetic material properties, especially for high flux densities and under DC biases, are vital parts of this project, and necessary for verification of the magnetic material models. So, first of all, the current hysteresis models should be extended to manage this task. Furthermore, that model must have the ability to be applied with a finite element or a reluctance network method. Power transformers have complex three-dimensional geometry with nonlinear materials in the core. These make it necessary to use powerful and accurate numerical methods such as finite element method to analyse and understand their behaviour. Nevertheless, this method is not efficient in terms of time and memory in practical design and optimization applications. Therefore, a fast method with promising accuracy is needed to replace it. Hence, developing a distributed nonlinear reluctance network model that can take into account the hysteresis model is intended in this project.
The main goals and expected tasks and achievements of the current work can be summarized as follows:

- Develop a proper hysteresis model to fulfil the requirement of the project.
- Establish a measurement setup in order to study core magnetic materials, obtain hysteresis model parameters and verify the models.

- Create appropriate three-dimensional nonlinear finite element models of various types of power transformers to study and understand how the DC magnetization functions.
- Develop a distributed nonlinear reluctance network model of power transformers with the capability to implement the hysteresis model and couple with a circuit.
- Study the interaction of the power transformer and the network.

1.3 Outline of thesis

The thesis is structured as follows:

- Chapter 2 gives a brief description of the theory of transformers and their structures. There are various transformer types and designs but in this chapter the emphasis is on the modern core-type power transformers.
- Chapter 3 is dedicated to measurement methods and challenges in the magnetic characterization of ferromagnetic materials. Since appropriate core modeling is essential for a comprehensive electromagnetic model of power transformers, the measurements are necessary for developing and verifying material models. The chapter begins with general information about the measurement of magnetic materials and continues by presenting the new control algorithm that is developed in this work. The algorithm is developed by the author of this thesis and is implemented in NI LabVIEW by Mr. Andreas Krings. The new method has considerable advantages in the measurement of the static properties of the magnetic materials.
- Chapter 4 and Paper I present the new differential scalar hysteresis model that is suggested by the author. The model is based on the classical Preisach theory of hysteresis. However, with its differential nature it inherits the advantages of the Jiles-Atherton model. The verification of the model has been done by measurements of the transformer core materials.
- Chapter 5 is concerned with the three-dimensional finite element model of power transformers. The various core types of single-phase and three-phase power transformers are modelled in this work by the author. The material is nonlinear and anisotropic and the windings are coupled to an external electrical circuit. The aim of modeling is to understand the effect of DC magnetization on power transformers. The simulation results and conclusion of the modeling are presented in this chapter. Also Paper II consists of a method for calculation of core

losses for power transformers especially with DC magnetization that is proposed by the author.

- Chapter 6 and Paper III introduce an efficient time step method for solving nonlinear reluctance networks that is developed by the author. Although the finite element method is a powerful tool to solve electromagnetic problems, its memory and time consumption prevent its use as a routine design and optimization method in practice. Hence, the reluctance network could supersede it. In fact, this chapter presents the first step towards developing a distributed nonlinear reluctance network method that it is intended to be developed in next phase of this project aiming of a PhD degree.
- Finally, Chapter 10 contains a summary, conclusion and the future works that will be done for the PhD degree.

Chapter 2

2 Basics of power transformers

2.1 Introduction

The enormous demand of energy is growing steadily due to industrial development and the increasing world population. This fact and environmental issues have heightened the importance of the production and transmission of electrical energy as a green and clear one. Nowadays, the majority of the electrical energy consumed is produced in power plants. This energy is produced and transmitted in the form of AC three-phase systems. An efficient transmission system is required to change the voltage level along it.
Power transformers are electrical devices that transmit the AC power based on the principle of induction [15]. They are employed in the power network to increase or decrease the voltage level with the same frequency. Figure 2.1 shows the schematic view of the electricity system from production to consumption [16].

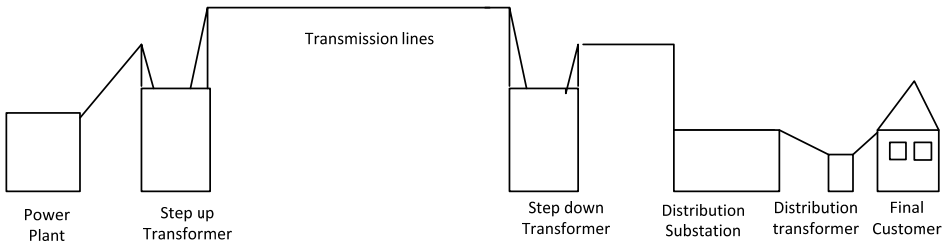

Figure 2.1. The schematic view of electric system from production to consumption.

Since the voltage level from the power plant to the distribution system changes several times, the aggregate of the installed power of the transformers usually

is about 8 to 10 times the capacity of generators in the power plants. Therefore, power transformers are one of the most vital components of the power network. They are usually expected to work for more than 30 years [17]. Hence aspects regarding power transformers including design, manufacture, protection, modeling, maintenance and diagnostics have substantial importance and have always been in the field of research interest [16].
This chapter begins with a brief explanation of the principles and theory of transformer working and then continues by introducing the structure of modern power transformers. A short description of various types of power transformers and their applications are given afterwards.

2.2 Theory of transformer function

2.2.1 Basic principle

A transformer is an electrical device that functions based on the induction principle. A simple transformer consists of two or more separate windings surrounding a common closed magnetic core which conducts the flux. Consider the simple transformer depicted in Figure 2.2. Faraday's law and Ampere's law can explain how a transformer works.

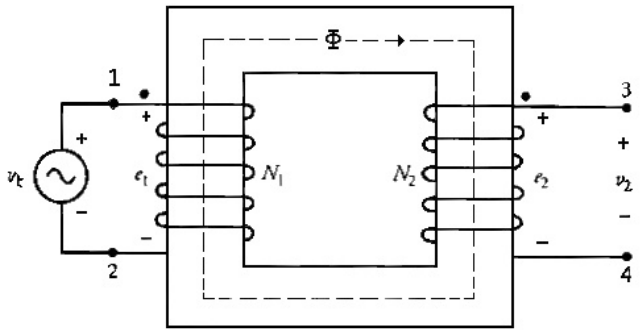

Figure 2.2. The principle of transformer working.

When a time-varying voltage is applied to the primary winding, it forces a flux to pass through it according to Faraday's law:

$$\lambda_1(t) = \int_{t_0}^{t} V_1(t)dt + \lambda_1(t_0) \tag{2.1}$$

, where λ and V are the linkage flux and induction voltage of the winding, respectively.

Since the core has a very high permeability compared with the surrounding air, the main part of the flux passes completely through the core which is called common flux. However, a small part of the flux passes through the air during its close path. This flux is called leakage flux or stray flux. Therefore, the time-varying linkage flux passes also through the secondary winding and again based on Faraday's law a time-varying voltage is inducted across it.

$$V_2(t) = \frac{d\lambda_2(t)}{dt} \tag{2.2}$$

Ampere's law in the integral form says that:

$$\sum NI = \oint H.dl \tag{2.3}$$

, where N , and I are number of turn and current of the windings, respectively. H is the magnetic field.

Therefore, if the secondary winding is open-circuit, only a current will pass through the primary winding that is proportional to the integration of the magnetic field along the closed path in the core. This current is called magnetization current. In fact, this is a current that is needed to make enough magnetomotive force (MMF) in the core to create flux regarding applied voltage. Hence, it is clear that the required current depends on the permeability of the material along the closed path.

In the case that secondary winding is connected to a load, it will carry a current, which is called load current. Thus, according to (2.3), a proportional load current will pass through the primary winding. In this way, the power is transmitted through the transformer based on the induction principle.

The core and the windings are perfect in an ideal transformer. In a perfect core the permeability is extremely high such that there is no leakage flux and the MMF required for magnetizing is zero. Also, resistivity in a perfect conductor is zero, which means that there is no resistive voltage drop along it. These conditions imply that the ideal transformer is loss-less. By applying these assumptions the relation of the voltages and currents of the windings can be obtained as:

$$\frac{V_1}{V_2} = \frac{N_2}{N_1} \tag{2.4 a}$$

$$\frac{I_2}{I_1} = \frac{N_1}{N_2} \tag{2.4 b}$$

Therefore:

$$V_1 I_1 = V_2 I_2 \Rightarrow S_1 = S_2 \tag{2.5}$$

In other words, the power is transmitted through an ideal transformer without any change. However, in practice, there is no such thing as a perfect core and windings. In order to derive a realistic electromagnetic model of transformers, the non-ideal properties of the core and winding and the effects of leakage flux should be taken into account. With respect to the core, nonlinearity, hysteretic properties, frequency dependent losses and core structure should be considered. For windings, frequency dependent losses, inductances, and capacitances are important. Of course, based on the aim and frequency range of the modeling, a suitable simplification can be implemented.

2.2.1.1 Losses in power transformers

According to routine tests of power transformers that are determined in the standards, the losses are classified into no-load and load losses [16]. No-load losses are measured when one winding is supplied with rated voltage and the other windings form open circuits. These losses always cause dissipation of energy whenever the transformer is connected to the network or not. Load losses or short-circuit losses are the active power absorbed by the transformer while carrying rated currents in the windings [18]. During this test, the high voltage winding is short-circuited, which result in a drastic reduction of the core losses.

However, the sources of the losses in transformers are core losses, winding losses, stray losses in metallic structural parts and insulation losses. Of these, the insulation losses are usually negligible in comparison with the others, especially under power frequency operation. The core losses create no-load losses and the load losses come from aggregation of the winding losses with the stray losses [16].

2.3 Transformer structure

2.3.1 Introduction

In detail, a power transformer has a complex structure with several components that can be listed as follows [19]:

- Tank
- Core
- Windings and insulation systems
- Leads and terminal arrangements
- Tap changer
- Bushing and current transformers
- Insulating oil and oil-preservation means
- Cooling system
- Constructional parts
- Protective equipment

In a common power transformer two or more separate concentric windings are wound on a limb of the magnetic core for each phase. The core, windings, metallic parts and tank are the components that can play a role in an electromagnetic analysis. So, they are described in more detail in the following sections.

2.3.2 Core

The core is the heart of the power transformer. It creates a closed magnetic circuit with minimum air gap and minimum magnetic reluctance in order to carry the linkage flux among the windings. The quality of the core plays an important role in the performance of transformers. Volt-per-turn, magnetization current and no-load losses are directly related to the design, material and building quality of the core [16].
On the other hand, low frequency transients in power transformers, such as inrush current occur due to the nonlinear and hysteretic properties of the core materials.
The core is stacked by a lamination of thin electrical steel sheets with a thickness of about 0.3 mm or less, which are coated with a very thin layer of insulation material with thickness of about 10-20 μm. This prevents large eddy current paths in the cross-section of the core [17].
With the development and on-going research nowadays, core materials are being improved with better core-building technologies. In the beginning of transformer manufacturing, core materials have inherent high losses and magnetizing currents. The addition of silicon to about 4 to 5% can improve the performance significantly, because it can reduce eddy losses and the ageing effects. The important stages of core material development are: oriented, hot-rolled grain-oriented (HRGO), cold-rolled grain-oriented (CRGO), and high permeability cold-rolled grain-oriented (Hi-B), and laser scribed [16]. Figure 2.3 illustrates the progress of core materials during recent decades.

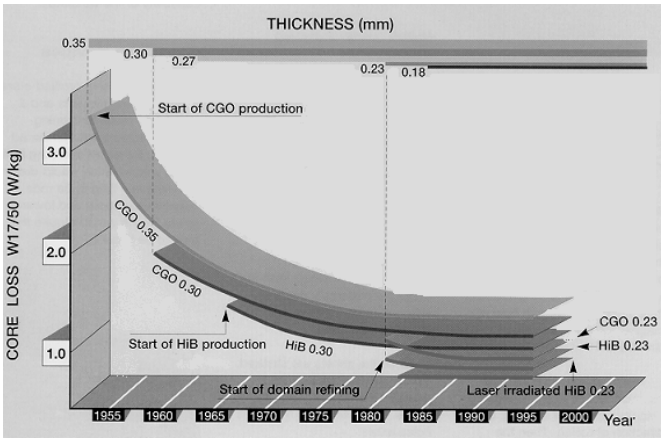

Figure 2.3. Core material progress along years.

Today, the materials used in power transformers are grain-oriented, which means that the magnetic properties are much better in the rolling direction than in other directions.

The core is made up two parts; limbs and yokes. Limbs are surrounded by windings and yokes connect the limbs together to complete the path of the flux. The place where limbs and yokes meet each other is called the core joint. The most common joint in modern power transformers is a mitred joint with a 45º cutting angle. Overlap length, number of steps and number of sheets per layer are the parameters of overlapping. According to the number of steps there are two types of core joints; overlap and step-lap. In the step-lap method, the number of steps is more than one and using up to five or seven steps is common [17]. Figure 2.4 shows cross sections of overlap and step lap joints. The quality of joints can affect the performance of the core.

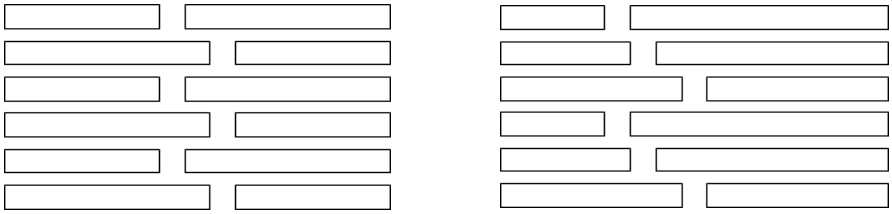

Overlap joint Steplap joint with three steps

Figure 2.4. Overlap and steplap joints.

Since the core limbs are surrounded by cylindrical windings, the circular cross-section of the core is ideal for the best utilization of space. However, to make a circular core with lamination of thin electrical steel demands a lot of time and labour, which increases the cost and time of manufacturing drastically. In practice, the core is given a stepped cross-section which approximates a circular one [20], as shown in Figure 2.5.

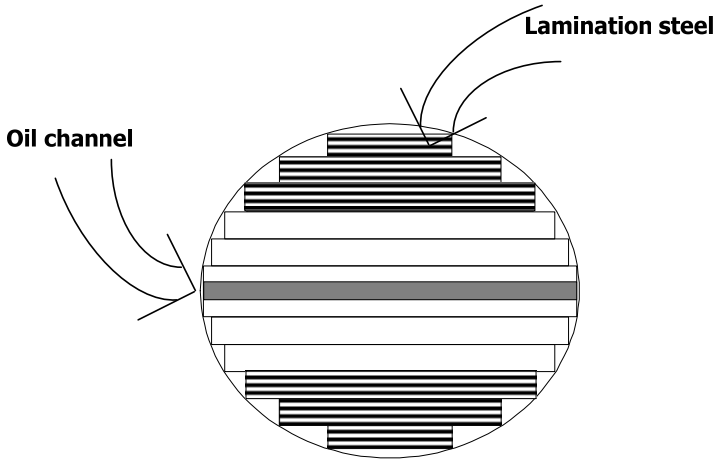

Figure 2.5. Core cross section.

2.3.3 Winding

Two main methods are utilized for winding the coils; layer winding and disk winding. In both of them the coil is cylindrical and the overall cross-section is rectangular. Figure 2.6 sketches these. Helical winding is another type, which is disk winding with two turns per disk. Each type has advantages that make it suitable and efficient in certain applications. The choice between them is made based on how well they function in respect of ease of cooling, ability to withstand over-voltages, mechanical strength under short-circuit stress and economical design [20].

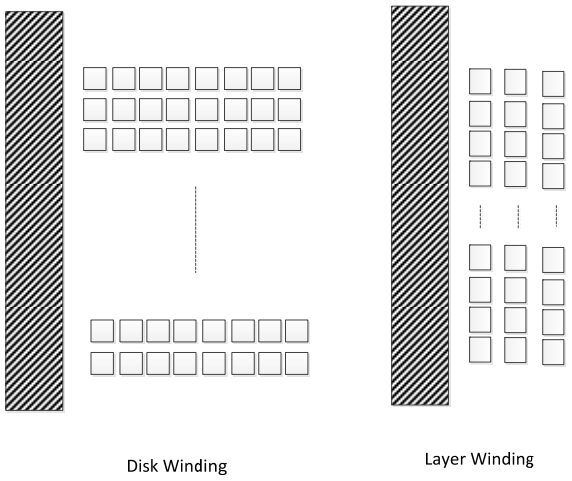

Figure 2.6. Disk winding and layer winding.

An insulated copper conductor with rectangular cross-section is used in windings of power transformers. Usually the conductor is subdivided with smaller strands in order to reduce the eddy current losses. In the case of employing a parallel conductor, they should be transposed along the winding to cancel loop voltages induced by stray flux. Otherwise, these voltages create circular currents, which impose extra losses. Continuously Transposed Cable (CTC) is used in the case of high power high current windings [16].

2.3.4 Construction

Apart from the core and windings, tank and core clamps are the structural parts that can be taken into account from electromagnetic scope.
The tank of power transformer is a container for the active part that is immersed in oil. The overall shape of it is rectangular cubic that is made of soft magnetic steel with a thickness of about a few centimetres. The tank is designed to carry out several tasks regarding mechanical, acoustic, thermal, transportation, electrical and electrometrical aspects [17].
From electromagnetic view point, especially with increasing rating and currents, the tank should minimize the stray fields out of transformer and eddy currents inside the tank. Eddy currents due to stray fields result in stray losses in the tank walls. In large power transformer, shielding is used to prevent stray fields in the tank wall. The shielding is done by mounting the laminations of copper or high permeable material on the inner side of the tank wall [16].

2.4 Transformer types

Power transformers are designed to manage the voltage level, power rating and application. Also, sometimes considerations of transportation and installation affect the design. Therefore, they can be classified with regard to each aspect. In this section, the classification is based on the construction of the core and windings [16].

2.4.1 Shell-form and core-form

From the construction type of the core and windings, the power transformer can be classified into core-form and shell-form [5]. In core-form transformers the windings are wrapped around the core with a cylindrical shape. However, in the shell-form design, the core is stacked around the windings that generally have a flat or oval shape and are called pancake windings. Figure 2.7 shows a three phase shell-form power transformer.

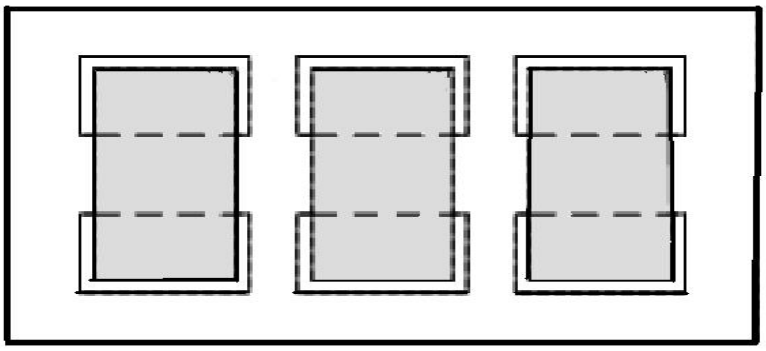

Figure 2.7. Shell-form three phase transformer.

The core-form design is widely used in power transformers. The reason is probably its better performance under short-circuit stresses. In this work, only core-form transformers are in the field of study.

2.4.2 Single phase vs. three phase

Providing a transformer for a three-phase system can be done in two ways; using one three-phase unit or a bank of three single-phase transformers. In the three-phase units there is magnetic coupling between phases while in a bank the transformers are magnetically independent. Each method has certain advantages over the other. The three-phase unit is more economical and costs

around 15% less than a bank of three single-phase transformers and occupies less space [16]. However, sometimes it is impossible to transport large three-phase power transformer units to the site and it is easier to transport three single-phase transformers. Another advantage of using a bank of three single-phase transformers is that, if one unit of the bank becomes out of order, then the bank can be run as an open delta connection. For these reasons, a bank of single-phase transformers is preferred for high power and high voltage units.

2.4.3 Types of core

Single-phase power transformers are usually made with two, three or four limbs, as sketched in Figure 2.8. For two limbs there is no return limb and the cross-section of the yoke is the same as the limb. With three limbs and four limbs there are two return limbs. The return limbs are not surrounded by any windings and their task is to create a closed pass for the flux. The cross-section of the yokes and the return limbs are a little bit more than half of the main limbs. As a result, the height of the transformer is decreased in comparison with the two limb version. On the other hand, in two limb and four limb cores, there are two limbs that are surrounded by windings. The connections of the windings of these limbs are parallel, which means the capability of carrying current is duplicated. As a result, for the same winding and the same voltage level the power of the transformer is two times greater. Therefore, the choice between these three types of core is based on the power and height limits regarding transportation.

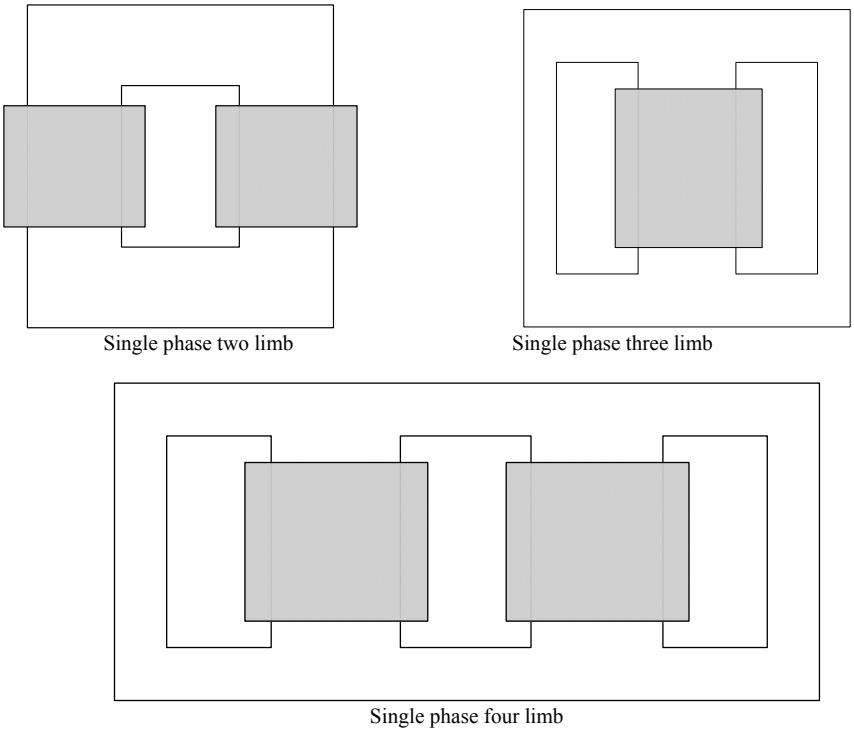

Figure 2.8. Core types of single phase power transformers.

Three-phase transformers have two types of cores; three limb and five limb, as illustrated in Figure 2.9 and Figure 2.10. In these cores there are three limbs that are surrounded by windings. Hence, in a three limb core, if at a time the algebraic summation of linkage fluxes in the phases is not equal to zero, a part of the flux has to close the path in air. The five limb core is used for large power transformers in order to decrease the height, stray fluxes and consequent eddy current losses.

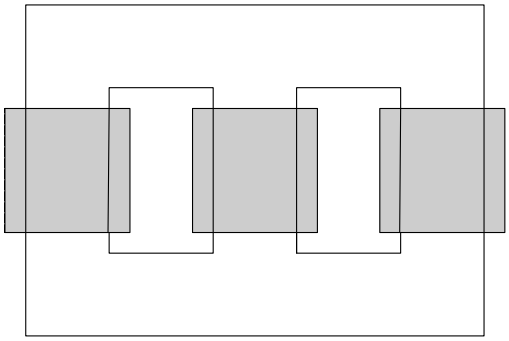

Figure 2.9. Three phase three limb core.

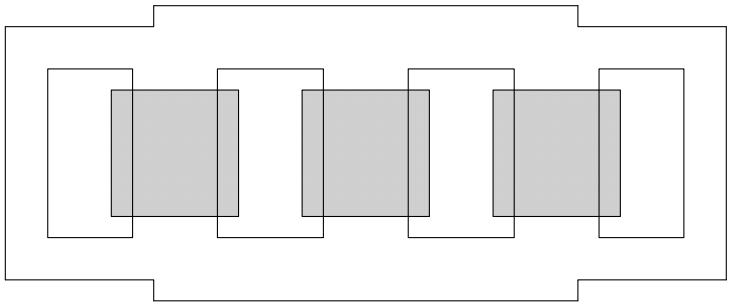

Figure 2.10. three phase five limb core.

2.4.4 Autotransformers

Autotransformers are types of transformers in which the primary and secondary windings have a common part and they are electrically connected at that common point [19]. This means that the power is transmitted using both galvanic and inductive methods. Reduced size and optimum use of materials are the advantages of these transformers. However, their low short circuit impedance and the direct connection of low voltage and high voltage windings prevent their widespread use in the network. They are more appropriate for applications where the voltage ratio is not so big and it is required to change the voltage level in small steps.

2.4.5 Special transformers

Rectifier Transformers, converter transformers for HVDC, furnace transformers and phase shifting transformers are special kinds of transformers

that are used in networks and/or in industry. Although, their main principle is the same as normal power transformers, their specific requirements and applications require special designs [21].

Chapter3

3 On the measurement of magnetic materials

3.1 Introduction

Today, magnetic materials are widely used in equipment which is essential for modern life. They have broad applications, from the generation and conversion of electrical energy to telecommunication, biomedical and information technology [22] [23]. Various types of magnetic materials exist. One classification divides them to soft and hard magnetic materials. Another one groups them in diamagnetic, paramagnetic and ferromagnetic [24]. In this work the focus is on soft ferromagnetic materials that are used in transformer cores.

The measurement of their properties is required in production, research, development, modeling and commerce [23]. They have magnetic, electric and mechanical properties. On the other hand, they also have microscopic and macroscopic properties. Therefore, in accordance with the aim of measurement and type of materials, special techniques have been developed and standardization has been introduced [22].

Regarding the scope of this work, the macroscopic magnetic characterizations of soft magnetic materials that are used in the core of modern power transformers are in the field of interest. The nonlinear and hysteretic properties of core materials have the most significant effect on the transient behaviour of power transformers in the low frequency range [25] [26]. Therefore, optimum design and appropriate electromagnetic modeling of transformers demands a good understanding of magnetic material behaviour. Measurements of magnetic material properties, especially for high flux densities and under DC biases, are vital parts of this project. They are also necessary for the verification and improvement of hysteresis models.

The control algorithm is the most important part of such a measurement system. Since the tested materials have nonlinear properties, and in order to achieve the desired flux density waveforms, control of the injected current is necessary [27]. Therefore a control algorithm based on local linearization has been developed in this work. The proposed method controls the rate of flux density. The algorithm functions very well for efficient demagnetization processes, measurement of anhysteretic curves, first-order reversal curves and any desired static hysteresis trajectory. Also, magnetization including a DC component is possible. The method is independent of small DC offsets of the current amplifier which exist in practice and can affect the measurements. The developed method has several advantages in comparison with former ones [27] [28] [29].
This chapter is dedicated to measurement techniques with emphasis on static properties. The principles of the measurement, definition of basic curves and properties and difficulties of measurement are described below. Eventually, the newly developed control algorithm that is implemented in a digital measurement system will be introduced.

3.1.1 What are the magnetic properties of materials

Magnetization, *M,* magnetic polarization, *J*, magnetic field intensity, *H* and magnetic induction or magnetic flux density, *B,* are the main magnetic quantities. From the viewpoint of electrical engineering, the magnetic characterization of a material determines how the magnetic polarization, *J,* changes with respect to the magnetic field intensity, *H,* in a certain condition. In fact, in ferromagnetic materials these macroscopic quantities are the results of an extremely complex sequence of microscopic processes. However, in the measurement the macroscopic outcomes are of interest. In the classical electromagnetic theory of continuous media, the magnetic field vector, **H**, is defined by the equation [23]:

$$\nabla \times (\frac{\mathbf{B}}{\mu_0} - \mathbf{M}) = \nabla \times \mathbf{H} = j_e \tag{3.1}$$

, where j_e is external current density. Thus:

$$\mathbf{B} = \mu_0 \mathbf{H} + \mu_0 \mathbf{M} \tag{3.2}$$

, where **B** is the magnetic induction vector in the material, **M** is the magnetization vector and j_e is the externally supplied current. The relation (3.1) shows that the magnetic field *H* is directly generated by the external

current. Also from (3.2) it is clear that **B** consists of two contributions; one from the magnetic field and the other from the magnetization. The second term is defined as the magnetic polarization vector, **J** [23]. Therefore, (3.2) can be re-written as:

$$\mathbf{B} = \mu_0 \mathbf{H} + \mathbf{J} \tag{3.3}$$

In the above equations, the **B** and **J** are in Tesla and **H** and **M** are in A/m.

In most ferromagnetic magnetic materials, the term of $\mu_0 \mathbf{H}$ is negligible in the interested range of **H**. As a result **B** is equal to **J**. Thus, one can say that the characterization of ferromagnetic materials basically implies the determination of the constitutive law **B(H).**

For a ferromagnetic material the relation of applied **H** and the magnetic induction is very complex and depends on the history of the material and the rate of magnetization. Therefore, the changing of **B** regarding **H** in a certain condition reveals special information about the intrinsic material properties.

3.2 Principle of measurement

Several techniques have been developed for the measurement of magnetic material properties, each of which is suitable for special applications. These methods, such as fluxmeteric techniques and magnetometric techniques, are used for magnetic properties. Other methods like force techniques, magneto-optical techniques and magnetostrictive techniques are employed for measuring other properties of the magnetic materials. The details of these methods are elaborated in [23] [22] [24].

In the measurement of magnetic properties, there are two main tasks. One is how to generate the desired *B* or *H* field, the other is how to measure these quantities. Thus, of the above mentioned methods, the fluxmeteric technique is considered in this work. In this method, the magnetic quantities of *B* and *H* are linked with electrical quantities of *V* and *I*, respectively. This method is founded on Faraday's law and Ampere's law. The principle of measurement setup is depicted in Figure 3.1.

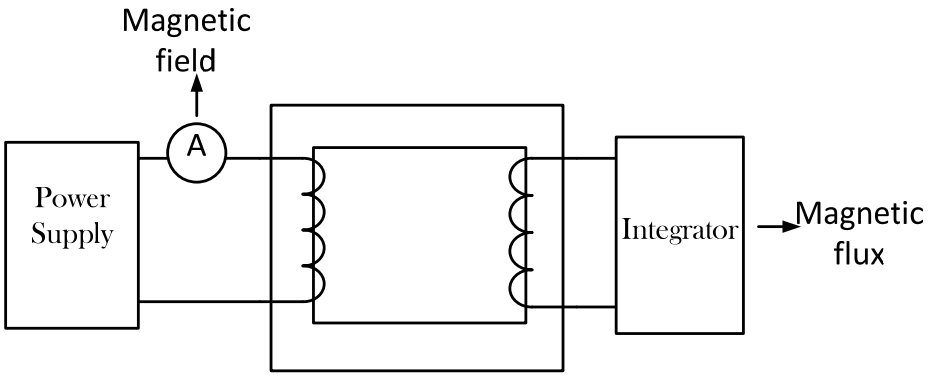

Figure 3.1. The principle of measurement by fluxmeteric method

In the method the test specimen is a closed magnetic circuit that is linked with two coils. The test sample is magnetized by the MMF that is generated by passing current through one of the coils. That coil is called the exciting coil and is connected to the power supply. The other coil is employed for the measurement of the induced voltage inside the sample. This open circuit coil is called the voltage coil.

The assumption is that the magnetic fields and the flux densities are uniform along the mean length path and inside the voltage coil, respectively. Therefore, the relation between the injected current and the magnetic field is obtained according to Ampere's law by:

$$H = \frac{NI}{l_m} \tag{3.4}$$

, where NI is the ampere-turn of the excitation winding and l_m is the mean length path.

Since the voltage coil is open circuit, there is no current passing through it. This means that the measured voltage across it is a pure inductive voltage. So, based on Faraday's law, the flux density, *B*, can be obtained by time integration of that voltage. Therefore:

$$B(t) = \frac{1}{NA}\int_{t_0}^{t} V(t)dt + B(t_0) \tag{3.5}$$

, where V is induced voltage and NA is the multiplication of the cross section of sample with number of turns in the voltage coil.

During the magnetization process of materials, one part of the energy is stored and one part of it is dissipated. The summation of areas of hysteresis loops comprising minor loops in a complete cycle is equal to the losses per cycle per unit of volume. This can be calculated by [22]:

$$W = \oint H \cdot dB \tag{3. 6}$$

,where W is the loss per cycle.

The trend to create a closed loop test sample and the linked coils has led to the development and standardization of several test methods. The most reputable ones are the Epstein frame test method and the single sheet test method that are described in detail in [30] and [31], respectively. Both of them have advantages and disadvantages. However, the Epstein frame method has greater traceability and reproducibility. A comparison between the methods and discussions regarding the challenges that each one deals with is presented in [32].

The Epstein test method is more accepted in the testing of transformer core materials [32]. Hence, this method is chosen for the measurements that have been performed in this work.

Today's evolution in digital technology, its advantages in acquiring and recording data and also its ability to implement complex control algorithms, have resulted in extensive control and measurement systems [22] [27].

Thus, the measurement system that is used in this work is a digital system.

3.2.1 Practical challenges of measurement

The measurement of soft magnetic materials shows some challenges as encountering practical problems regarding measurement sensors and providing the excitation current. Since the input of digital data acquisition systems should be voltage signals in a certain range (usually between ±1v ±10v), all the measurement sensors should provide a voltage proportional to the measured signal in their outputs. Also, the problem of noise is always annoying, especially when the measurement signal is very low. In order to prevent aliasing error, the sampling frequency, according to Nyquist's theory [33], should be at least two times greater than the highest frequency that it is intended to measure.

Digitally recorded data usually needs some signal processing and de-noising. These processes can be done offline; however, when the measured data is required as an input of the control systems, the processes should be performed online. This task depends on the digital system characteristics and the complexity of processes might cause some difficulty and require special consideration in the implementation of the control systems. On the other hand,

the safety conditions and prevention of the creation of grounding loops should be taken into account in the connection of the digital system and power circuits.

To achieve the aim of higher precision in the digital measurements of analogue signals, the range of the output voltage of the sensors must be as close as possible to the input range of the data acquisition card. In fact, that voltage should be proportional to the real quantity that is measured by the sensor. The variation of the magnetic field, from the low flux density region to the saturation region, is very big for soft magnetic materials. However, the precision of the measurements in both areas is important. Especially, the problem of environmental noise increased when the signals are smaller. Therefore, selection of a sensor that is accurate enough in the range of the measuring current and frequency is very important. In our experience, a high accuracy shunt resistor for this application is better than a Hall Effect sensor or clamped current sensor since it can function easily from DC to several kHz.

There are two options for integration of the induced voltage from a voltage coil to obtain the flux density: an analogue integrator or a digital integrator. A high accuracy digital integration demands a high sampling rate according to the measurement frequency and it is necessary to use filtering and other signal processing procedures. Analogue integration, however, can be done by using RC or RL circuits. The analogue integration usually needs to be amplified before connection to the digital data acquisition device, especially for low frequency measurements. The circuit of the analog integrator is shown in Figure 3.2.

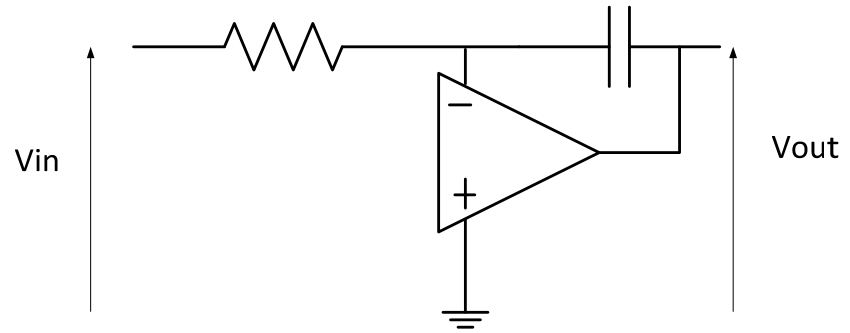

Figure 3.2. The circuit of analog integrator.

The main problem when measuring flux density is the problem of noise. Even with only very small noise in the voltage signal. Its integration with time still results in a significant error. Therefore, for noise cancellation a digital calibration method is employed. In this method at first when there is no input

signal the average slop of the recoded flux density is calculated. It can be done by recording the flux density at two instances with an interval of a few seconds. The ratio between the flux variation and interval time gives the average slop. Then, at the next time step, a growing signal with the same slop is subtracted from the measured signal of the flux density.

The power supply could be a controllable voltage or current power supply with a control signal. Also, in higher precision power supplies the existence of a small DC offset in the output is unavoidable. Since, the voltage offset can saturate the sample after a while, a controllable current source was preferred in the measurement systems. However, the current offset in the output of the current source is a reason for error and causes unwanted magnetization. In [27] a transformer between the power supply and the test frame is used to remove this offset. However, this method has limitations for DC measurements. This can also be composite with a signal that is generated for the control of the amplifier. The proposed algorithm in this work is not sensitive to the current offset.

As the requirements of the standards [30] [31] and also for research purposes a controlled magnetization process is necessary for the measurement. Figure 3.3 shows a measured hysteresis loop with at a very low frequency (50 mHz) sinusoidal magnetization current and a corresponding loop obtained by use of the controlled magnetization rate method.

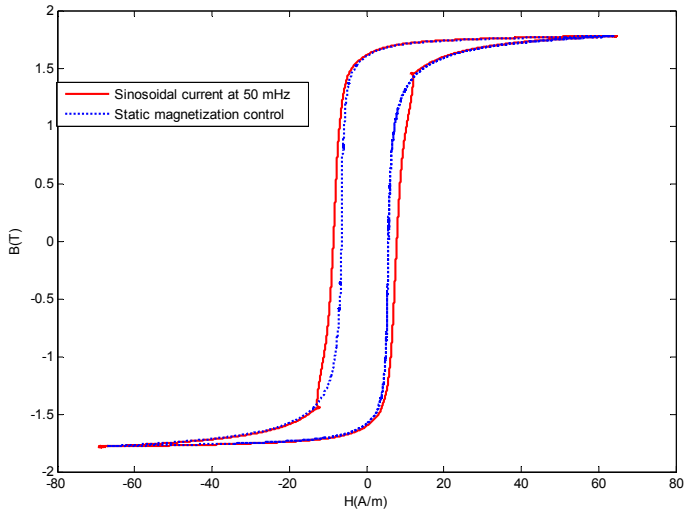

Figure 3.3. Comparison between measured static hysteresis loop with different methods.

3.2.2 Control algorithms

The ability to make accurate measurements of symmetric and asymmetric static hysteresis loops, initial magnetization curves, anhysteretic curves and first-order reversal magnetization curves is very important for understanding the behaviour of the magnetic materials and for obtaining the parameters used in hysteresis models.
For accurate, reliable and efficient measurements of the abovementioned properties, a controlled magnetizing process is required. The rate of magnetization should be as low as possible, such that dynamic effects become negligible.
Because of the nonlinearity of the magnetic materials, a closed loop control must be used in the measurement system. However, there exists no general method for control of closed loops [27].
In conventional analogue systems a negative feedback is used to obtain the desired magnetization waveform. However, due to the limitations of analogue feedback, this method does not work properly in the case of high flux densities or high permeability magnetic materials [27].
Since the progress in digital control and great capabilities regarding programming, recording and creating user interface software, most of the new measurement systems are based on digital technology. Thus, in the previous works [27] [28] [29], some methods are proposed for digital control systems in order to magnetize the material by a desired periodic flux density waveform. The main concept in these methods is to modify the magnetization current waveform iteratively for each period until a desirable magnetic flux density waveform is reached. In practice, the correction is carried out off-line between two iterations.
Although these methods are suitable for measurements in the power frequency range and for high frequency application, they have serious limitations that make them inappropriate for static (very low frequency) applications. The methods are very time-consuming at low frequencies, e.g., several hours in the range of 0.5 Hz [27], which can also cause measurement error of the flux density, as mentioned in 3.2.1. Besides, they only work for periodic flux density waveforms. Therefore, they are not applicable for the demagnetization process and anhysteretic curve measurements with a controlled flux density waveform. Furthermore, they are restricted to peak flux density values up to only 90% of saturation [27]. Measurement with DC magnetization is not possible in the iteration-based method.
In this work, we introduce a novel control algorithm that has been developed and implemented for static measurements. In the next section the method will be described in detail.

For measurement at power frequency and higher harmonics with sinusoidal flux density waveform, the method that is presented in [] is implemented.

3.3 Proposed measurement method

3.3.1 Test setup

The control algorithm described later is implemented on a National Instruments CompactRIO system consisting of a Power PC (NI-9022) running the LabVIEW real time operating system (RT System) and an FPGA (NI-9114) for controlling the I/O modules. A block diagram of the measurement setup is shown in Figure 3.4.

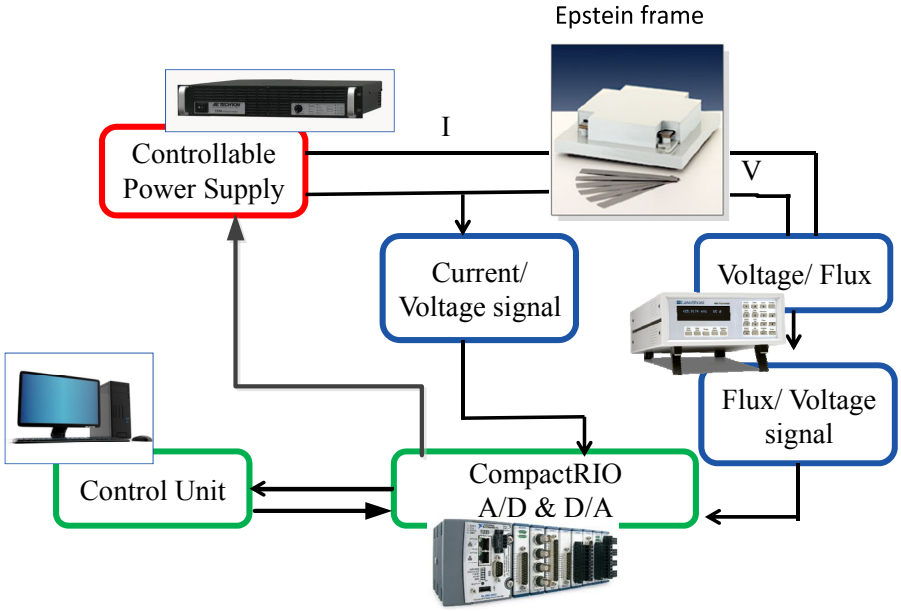

Figure 3.4. The block diagram of the measurement setup.

The main power supply is a controllable current source, AE Techron 7224 power amplifier, which is controlled by an input voltage signal. The proposed control algorithm that is implemented in LabVIEW determines the input voltage that is fed into the power supply. The voltage is generated by an analogue output channel of a National Instruments DAQ card. The current is measured over a high precision shunt resistor of 1.2 Ohm connected in series with the excitation winding and the amplifier. The flux density is determined by a Lakeshore 480 Fluxmeter, which integrates the voltage of the

measurement winding. The measured signals are used as the input of the control algorithm.

3.3.2 Algorithm (LLM)

3.3.2.1 Initial calibration

As mentioned before, an integration of the voltage is required to obtain the magnetic flux density. However, in fact we only can get the change of the magnetic flux density from the time instant when the integration is started. It means that to obtain the value of flux density, a reference point is necessary since the current situation of the material depends on the past history. Thus, the reference point should be independent of the history. Such a point could be the origin or the saturation point. The origin point is reachable after performing the demagnetization process [23] and at that point B and H are equal to zero and the magnetization of all domains compensate each other. Nevertheless, at saturation points all domains are oriented in the same direction. The saturation point method is employed in this work to achieve the value of the flux density. If the magnetic field, H_s, takes the material to the saturation region the magnetic flux density would be B_s. In that case by applying $-H_s$, due to the symmetry properties, the material goes to the saturation region in the opposite direction and the flux density would be $-B_s$ in turn.

The employed algorithm works based on this fact. First, a sinusoidal current with very low frequency in the order of 0.05 Hz is applied to the material. The amplitude of the current should be enough to take the material to saturation at the peak points. Hence, the real value of the flux density, B_{real}, can be calculated by:

$$B_{real} = B_{meas} + \frac{B_{\max,meas} + B_{\min,meas}}{2} \tag{3.7}$$

, where B_{meas}, $B_{\max,meas}$ and $B_{\min,meas}$ are the measured flux from the fluxmeter, measured flux at maximum H and measured flux at minimum H, respectively. Figure 3.5 depicts the calibration process. It should be noted that the fluxmeter is calibrated before starting the measurement.

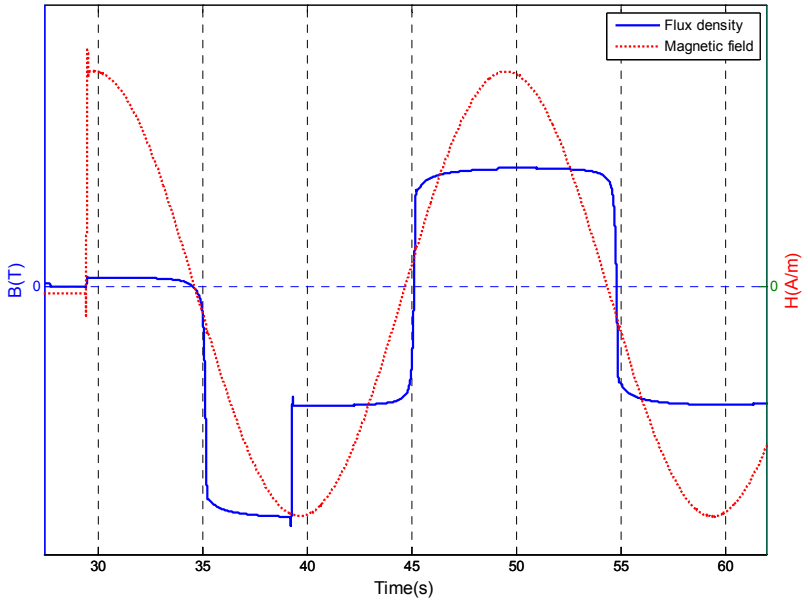

Figure 3.5. Initial calibration process of the measured flux density.

3.3.2.2 Main part

The aim of the control algorithm is to control the magnetization of the materials. For instance, for the static measurements, magnetizing with constant and very small (*dB/dt)* generally is required.

The concept of the control algorithm to perform this task is to determine the output voltage of the DAQ at each time step in order to create an excitation current that magnetizes the test sample according to the reference value of the flux density rate, $(dB/dt)_{ref}$. In general, the reference value can be constant or a function of time.

The main idea in developing a control algorithm is that the control algorithm should predict or estimate the (*dH/dt)* for the next step. If the change of the magnetic field at each step is small enough one can assume that the magnetization trajectory is linear. Thus, the required change of magnetic field can be obtained by:

$$\frac{dH}{dt}^{n+1} = \left(\frac{dB}{dt}\right)_{ref} \cdot \frac{\Delta H}{\Delta B}^{n} \tag{3.8}$$

, where n and Δt are the step number and time step of the algorithm. Therefore, at the time t, the *(dH/dt)* that is required in order to magnetize the

sample with $(dB/dt)_{ref}$ during the next step of the algorithm is known. Thus, during the step the control signal of power supply is linearly growing with a slop proportional to the obtained *(dH/dt)* at time *t.* At the end of time step $(t+\Delta t)$, the new value of $(\Delta H / \Delta B)$ is calculated in order to achieve *(dH/dt)* for the next step according to (3.8). This procedure continuous for the next steps. We call this method Local Linearization of the Magnetization (LLM).
In fact, the proposed control algorithm is an open loop system. This method has several advantages over other digital control methods [27]- [29], especially in the measurement of static properties. Its benefits can be expressed as follows:

- It can control the flux density rate with an extremely low rate of magnetization.
- It is not sensitive to small offsets of the power supply.
- It can be used in creating the desired hysteresis trajectories.
- The demagnetization process and the measurement of anhysteretic points become efficient.

Implementation of this method involves several complex considerations in practice. The condition during the initialization of the algorithm, the selection of the increment between successive time steps, and the calculation of *dH/dB* at each time step play important roles regarding the stability and efficiency of the method.
In the currently implemented work the absolute value of reference *dB/dt* can be determined by the user.
After initial calibration cycles, the algorithm starts to work. For the first few steps, the change of the magnetic field is constant and very small. These steps are necessary to ignite the control system and provide the value of (*dH/dB*) for the next steps. This period is called the transition time.
As mentioned before, noise is always excited in measured signals. Therefore, estimation of *dH/dB* is a tricky task. The time step for calculation of *dH/dB* should be big enough for the absolute value of *dB* to increase until the noise can no longer affect the calculations. This means the time step of the control system can be much higher than the sampling time of the DAQ. This issue is illustrated Figure 3.6.

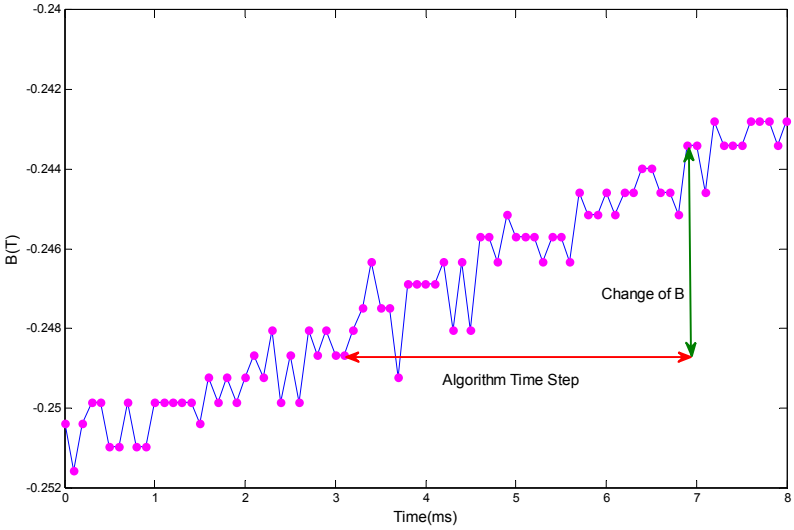

Figure 3.6. The effect of noise and selection of proper time step for the algorithm.

The transition time, using constant or adaptive time steps and the calculation method of *dB/dH* are matters through which the method can be modified or improved.

3.3.2.3 GUI

Figure 3.7 shows the Graphical User Interface (GUI) of the implemented algorithm in LabVIEW.

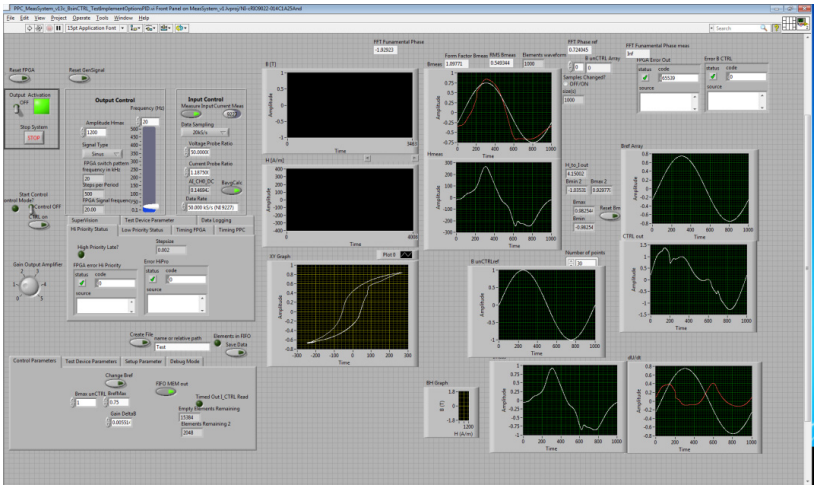

Figure 3.7. The GUI of the implemented algorithm in LabVIEW.

This GUI gives the possibility to the user to set the parameters, adjust the frame properties, and control the process of the measurement and save the measured data.
Also, the dedicated subroutines are available for demagnetization, measurement of anhysteretic points and the first order reversal curves.

3.3.2.4 Examples of measurements

The implementation of the proposed method and tests with several samples has demonstrated its great features for static measurements. Figure 3.8 shows a number of measured symmetric hysteresis loops. In Figure 3.9 the static hysteresis loop with a DC bias is illustrated. In Figure 3.10 -Figure 3.13 the measured loops and flux and magnetic field waveforms of a demagnetization process are presented.

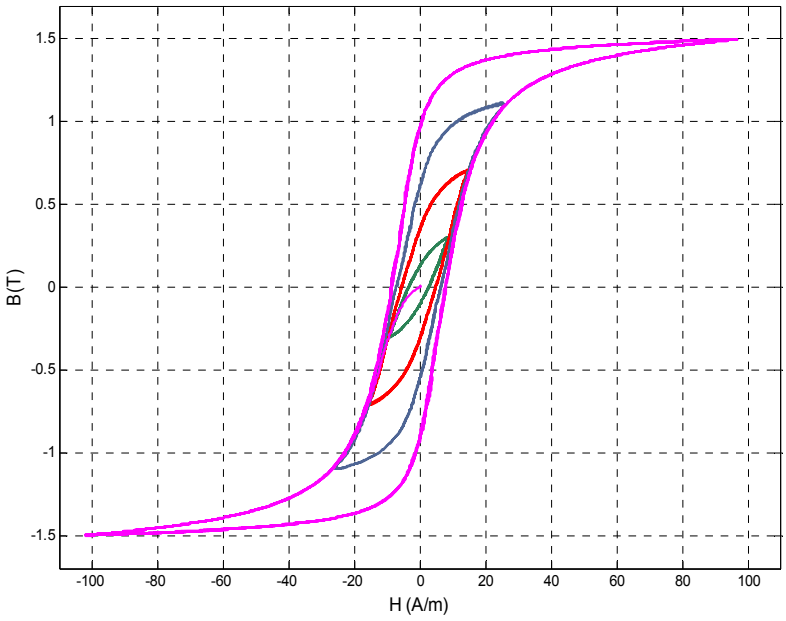

Figure 3.8. Symmetric static hysteresis loops.

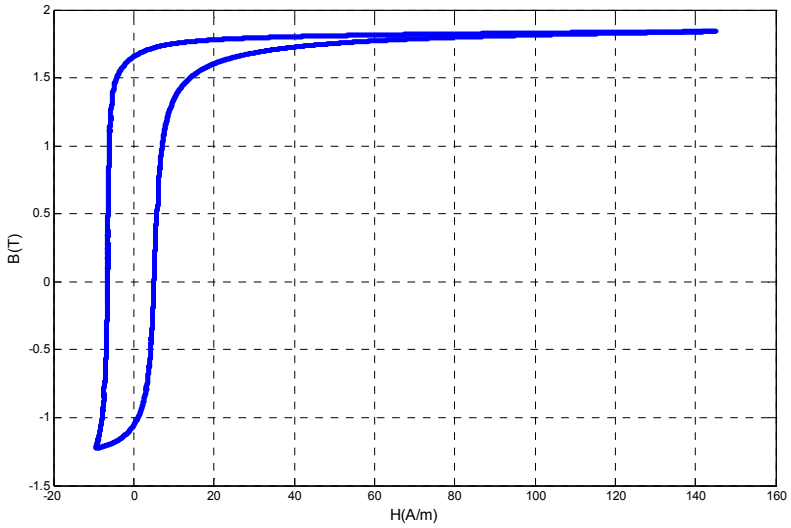

Figure 3.9. Hysteresis loop with DC bias.

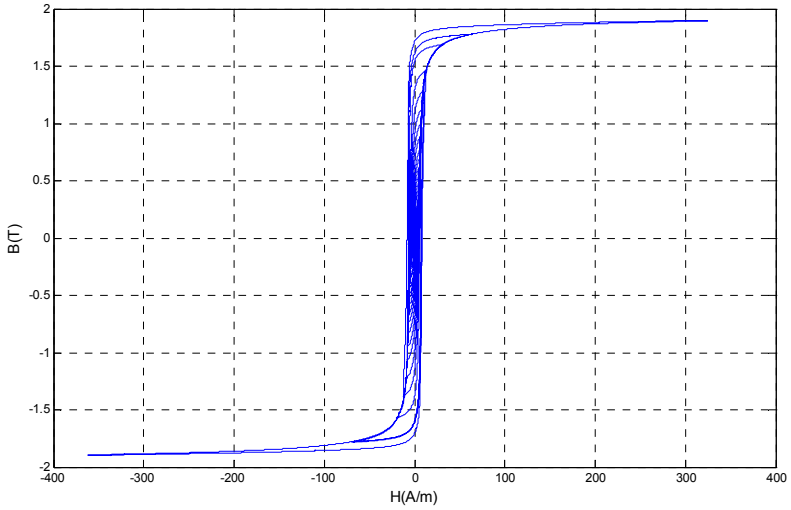

Figure 3.10. Hysteresis loops during the demagnetization process.

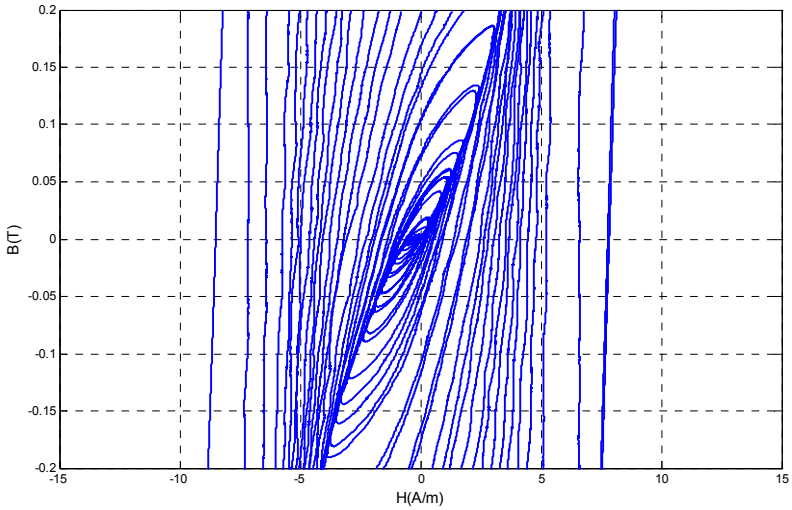

Figure 3.11. Zoomed demagnetization process around orgin.

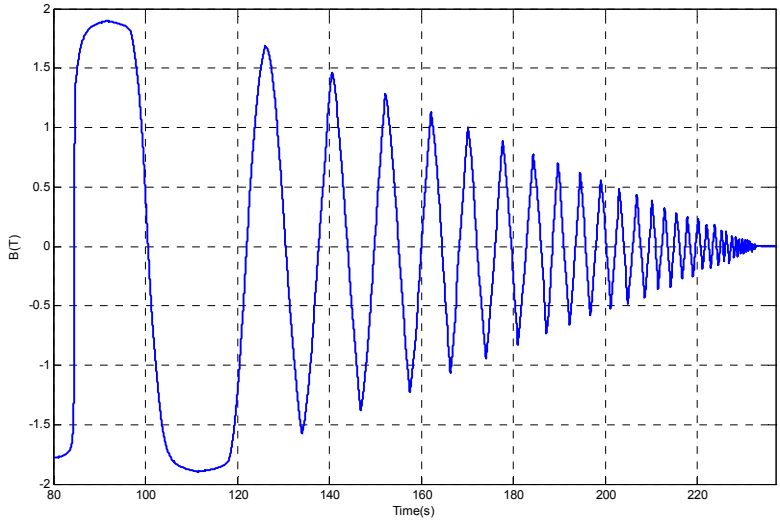

Figure 3.12. Flux density waveform during demagnetization.

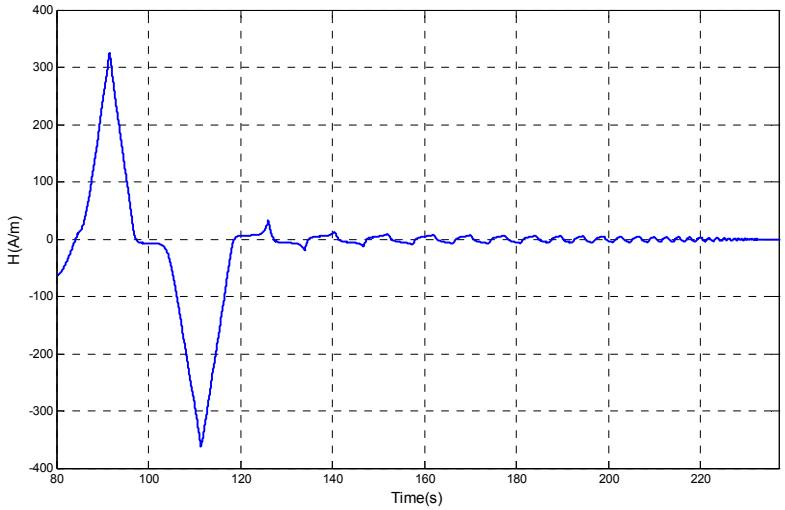

Figure 3.13. Magnetic field waveform during demagnetization.

3.4 Measurements of the anhysteretic curve

The anhysteretic curve of a ferromagnetic material constitutes the "ideal" magnetization curve of the material if it were perfect, in the sense that it has no defects or other deficiencies that hinder the magnetization and demagnetization process. To create accurate models that describe the magnetic hysteresis originated by the abovementioned causes, it is of great value to be able to distinguish between the intrinsic magnetization of the material itself and the magnetization effects that are caused by structural conditions and defects. This "ideal" so-called anhysteretic curve plays a vital role in the well-known hysteresis models such as the Jiles-Atherton [34] and Bergqvist lag model [35]. The ordinary method used to reach each point of the anhysteretic curve involves subjecting the material to an alternating magnetic field that decreases gradually simultaneously with a superimposed bias DC field. The descending field must also start from a saturated state of the material. Therefore, by using a repeatable process the obtained points are independent of the previous memory of the material. Hence, the anhysteretic curve is a single valued function of the applied bias DC field. Figure 3.14 and Figure 3.15 show the example of the B and H field with respect to time for measurement of one point on the anhysteretic curve by using a decreasing alternating field described in [36].

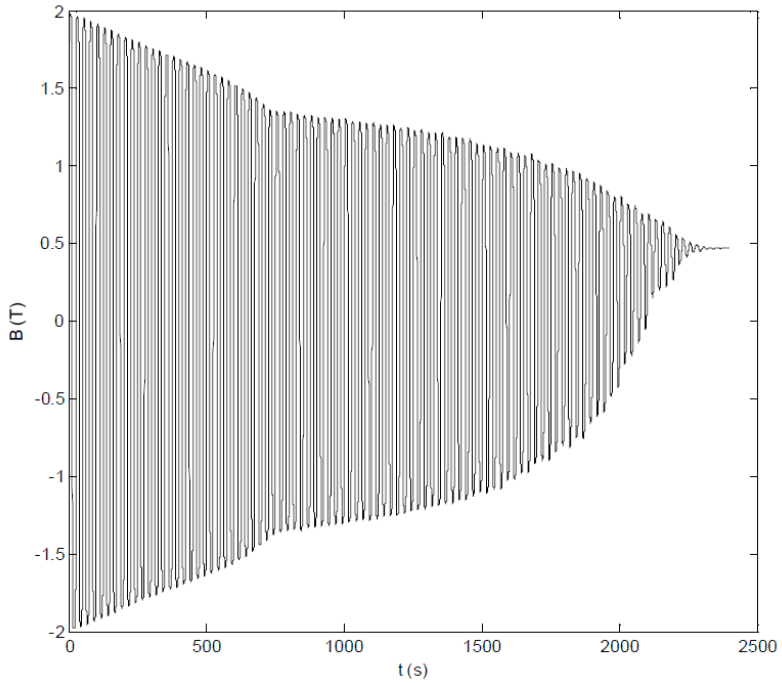

Figure 3.14. *H*-field during measurement of one point on anhysteretic curve, adapted from [36].

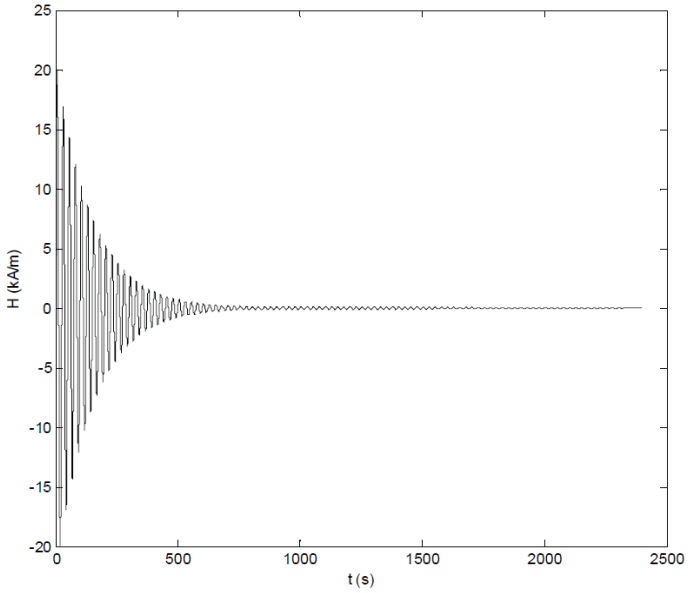

Figure 3.15. *B*-field during measurement of one point on anhysteretic curve, adapted from [36].

As can be seen from Figure 3.14 and Figure 3.15, this method takes a lot of time, of the order of a couple of hours, to measure one point. Besides the long time required, this leads to error in the measurement of flux density because of the existence of noise. This error is described in 3.2.1. Another problem is that the fast step-down near the final point can affect the accuracy of the measurement. This occurs because of the nonlinearity of the material and the *H* field control instead of controlling the *B* field. Also, the small offset of power supply is another source of error in this method.
This work presents a method based on a controlled flux density waveform instead of a magnetic field waveform to overcome these problems.
The applied waveform is a decreasing flux density waveform around a DC flux density instead of a DC magnetic field. This task can easily be performed using the introduced control algorithm. Examples of *B* and *H* waveforms and the corresponding hysteresis trajectory used to obtain the points on the anhysteretic curve are shown in Figure 3.16 - Figure 3.17.

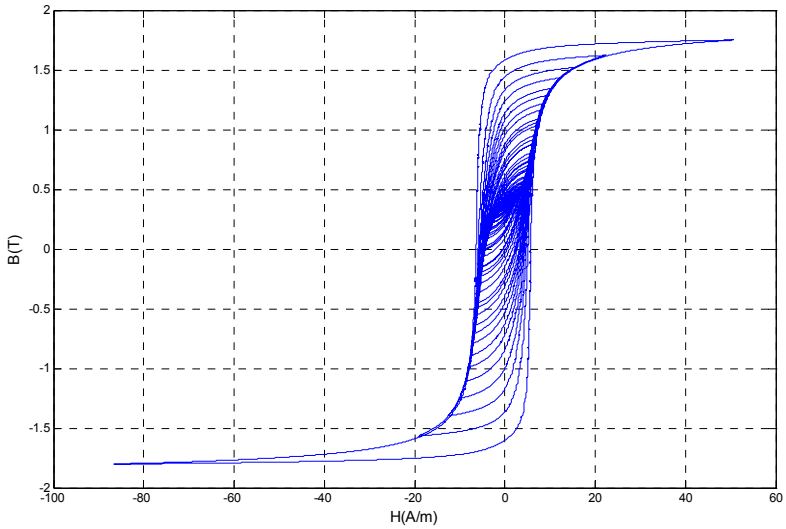

Figure 3.16. Hysteresis loops during measurement of anhysteretic point with 0.4 T DC offset of B by using the new method.

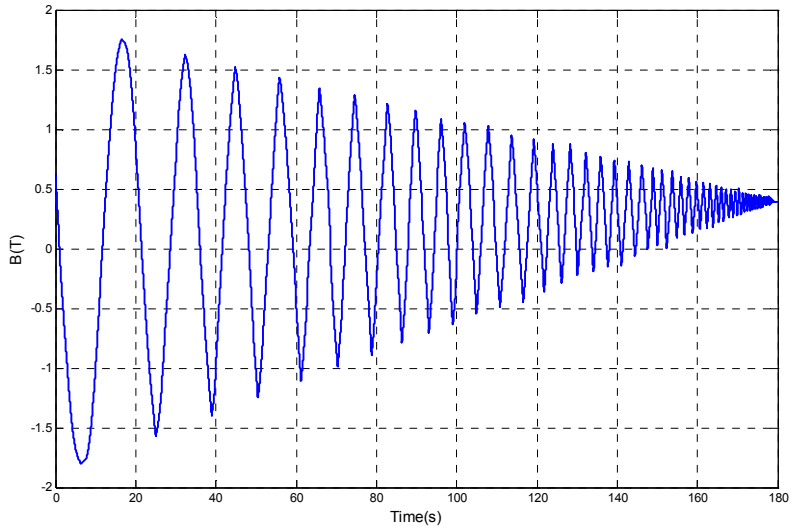

Figure 3.17. B-field during measurement of the anhysteretic point with 0.4 T DC offset of B by using the new method.

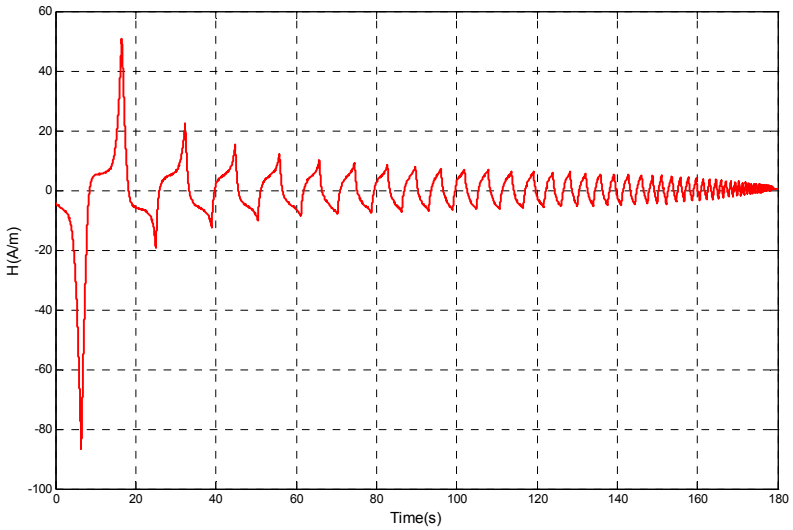

Figure 3.18. H-field during measurement of anhysteretic point with 0.4 T DC offset of B by using the new method.

It can be seen that the measurement time decrease to a few minutes and the rate of change of flux density is under control. Figure 3.19 and Figure 3.20

show the measured anhysteretic curve with major loop and initial magnetization curve, respectively.

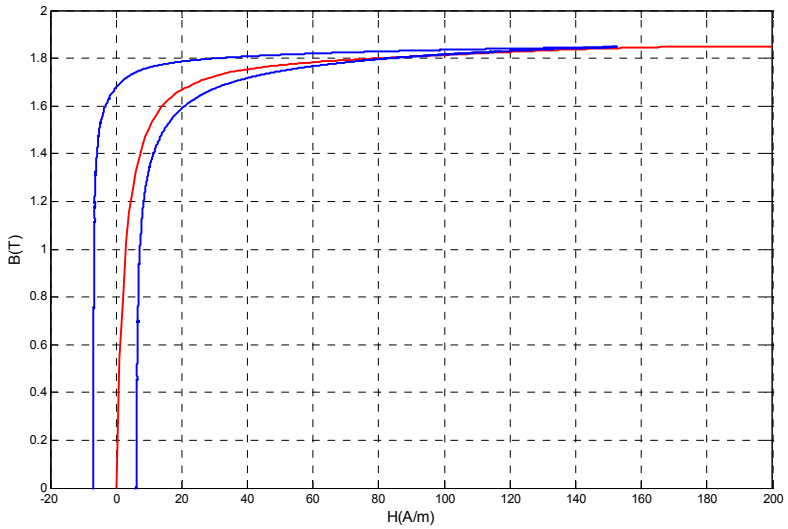

Figure 3.19. Anhysteretic curve with major hysteresis loop.

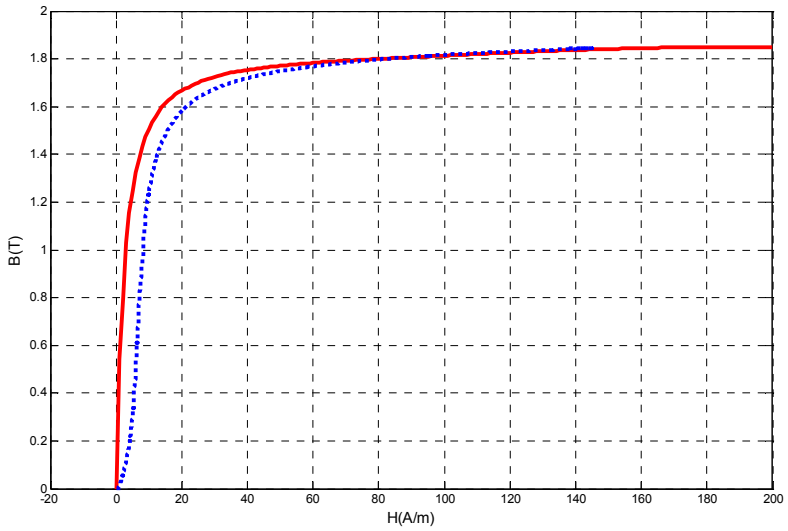

Figure 3.20. Anhysteretic curve with initial magnetization curve.

Chapter4

4 Hysteresis Modeling

4.1 Introduction

The magnetization is proportional to the applied magnetic field in linear materials such as air. In contrast, there is complex relationship between these quantities for ferromagnetic materials. Any point of (*M, H*) can be traversed in a trajectory that is related to the past history of the material [23]. This is because of a property that is called hysteresis. Therefore, the relation between magnetization and the magnetic field for ferromagnetic materials is history-dependent [37]. In other words, these materials have a memory of past events. In fact, this behaviour is the result of an extremely complex set of microscopic processes such as domain wall motion, domain structure rearrangement and rotation of magnetic moments [23]. However, obtaining the relation between the macroscopic quantities is of interest.

Therefore, the aim of a hysteresis model is to predict how the magnetization, magnetic polarization and the magnetic flux density change with the applied magnetic field *H*. However, as mentioned in section 3.1.1, magnetization *M*, magnetic polarization *J* and magnetic flux density *B* have a simple relationship with each other. This means that if one of them is known the others can be calculated easily by:

$$B = \mu_0 H + \mu_0 M = \mu_0 H + J \tag{4.1}$$

Hence, one can say that hysteresis modeling is the determination of the constitutive law of *M (H), J (H)* or *B (H)*. Over the years, different hysteresis models for different applications have been suggested and modified. Some good reviews of these can be found in [35] [38].

Based on Bertotti's theory [39], the hysteresis trajectories can be decomposed to static and dynamic components. The dynamic component is created due to eddy currents depending on the rate of magnetization. This part can be

formulated by solving Maxwell equations [39]. The static component is rate-independent and carries the hysteretic properties. In fact, the main task of a hysteresis model is to model the static component.
Also, the hysteresis models can be grouped into scalar hysteresis and vector hysteresis [35] [37]. In the scalar model the input and output of the model are scalar variables, while they are vectors for vector hysteresis models. The models can be established based on the physical interpretation of the phenomena or they can be based on pure mathematical fitting on experimental data [35]. For analysis purposes, some models may perform better than others. For example, in order to investigate the effect of temperature or stress on a material, the Jiles-Atherton model seems to be suitable. For vector hysteresis modeling, the Bergqvist lag model and other play operator based models may be more appropriate [35].
Accurate electromagnetic analysis of devices comprising magnetic materials such as transformers and electrical machines requires an appropriate hysteresis model. An ideal model for analysis of electromagnetic transient phenomena such as inrush currents, ferroresonance and DC magnetization that have complex hysteresis trajectories must fulfil the following features:

- Accurate prediction of the hysteresis trajectory in symmetric and asymmetric minor loops and in the saturated region.
- The *B* field should be the input and *H* field the output of the model.
- The model should be based on a direct mathematical relationship and not on a composite algorithm.
- It should be possible to estimate the model parameters from minimal and easily accessible measurement data.
- Fast, and not memory-consuming.

The Jiles-Atherton (J-A) model, because of its differential nature, is easy to implement, but its accuracy predicting minor loops is not good [38]. Among the current models, the Preisach theory is widely recognized as the best for modeling static scalar hysteresis, especially for accurate prediction of minor loops [37]. However, among the features of the ideal model mentioned above, the classic Preisach only has the first one. Thus, over the years, researchers and engineers have attempted to find solutions to improve this model for practical use.
In this work, a differential scalar static hysteresis model is introduced. This model can cover the advantages of both the J-A and Preisach models, while avoiding their disadvantages. The experimental verification proves promising performance of the model.
Thus, in this chapter a brief description of the J-A and Preisach models is presented. Then the new model is introduced.

4.1.1 J-A Model

The original Jiles-Atherton theory was first introduced in 1984 [34] in order to describe scalar hysteresis and it has been further refined and investigated by several researchers [40] [41] [42] [43]. In this model, which is based on the physics of domain wall motion, the magnetization of ferromagnetic materials M is decomposed into its reversible M_{rev} and irreversible M components:

$$M = M_{irr} + M_{rev}. \tag{4.2}$$

The reversible component is approximately proportional to the difference between the anhysteretic, M_{an}, and the irreversible magnetization:

$$M_{rev} = c(M_{an} + M_{irr}) \tag{4.3}$$

, where c is a material constant.

The effective magnetic field, H_e that is experienced by individual magnetic moments is equal to:

$$H_e = H + \alpha M \tag{4.4}$$

, where α is a constant that represents inter-domain coupling.

So, the effective magnetic flux density can be obtained by:

$$B_e = \mu_0 H_e \tag{4.5}$$

According to the equality of the supplied energy with the summation of stored and dissipated energy, it can be shown that:

$$\frac{dM_{irr}}{dH_e} = \frac{M_{an} - M_{irr}}{k\delta} \tag{4.6}$$

where δ is a directional parameter that is equal to +1 if $dH/dt > 0$ or is equal to −1 if. $dH/dt < 0$ However, k is a material parameter that depends on pinning sites in the material. Thus, bigger k results in bigger hysteresis losses. This parameter can be estimated as a constant, though it can vary with current M and H in the more general model. The (4.6) can be rearranged as:

$$dM_{irr} = \frac{M_{an} - M_{irr}}{k\delta - \alpha(M_{an} - M_{irr})} dH \tag{4.7}$$

Therefore, by substituting (4.7) in derivative form of (4.3), the relation between magnetization and the magnetic field can be written as:

$$\frac{dM}{dH} = (1-c)\frac{M_{an} - M_{irr}}{k\delta - \alpha(M_{an} - M_{irr})} + c\frac{dM_{an}}{dH} \tag{4.8}$$

The anhysteretic magnetization is given by the Langevin function as:

$$M_{an} = M_s(\coth\frac{H_e}{\alpha} - \frac{\alpha}{H_e}) \quad (4.9)$$

, where M_S is the saturation magnetization. However, this approximation is not valid for all materials [35], especially for oriented steels that are used in transformer cores.

Although the J-A model is a well-known model that is implemented in the finite element method [44] and electrical circuit simulation software such as EMTP [45], it has some problems and difficulties in practice.

The inherent problem is that the minor loops in general are not closed and the accuracy of the prediction of a complex hysteresis trajectory is not so good [35]. A modification has been proposed in [46] to get over this problem. But this makes the model very complicated. Also, in [43] an inverse model of J-A is suggested, but it is based on approximation of the anhysteretic magnetization according to (4.9).

Although the parameters of the model have physical meaning, they should be obtained from measurement data. So far, several methodologies have been used regarding efficient estimation of the parameters. The performance of the model is very dependent on the accuracy of the estimated parameters. Also, in [47] it is shown that the parameters can change with the magnetic field.

4.1.2 Preisach Model

The Preisach model originally was introduced by Z. Preisach in 1935 [48]. It was a physical model for ferromagnetic hysteresis, but its application was extended to mechanics and superconductivity [35]. The model has been widely modified over the years by researchers [37]. The model was presented in purely mathematical form and a representation theorem of it was derived [37]. The model has also been extended to vector hysteresis modeling [37]. In this section, the Preisach model for static rate-independent scalar hysteresis is considered.

The classical Preisach model describes magnetic materials by using a high number of hysteresis elements or hysteresis operators that also are called delay operators or thermostat hysteresis operators [35]. A hysteresis operator is depicted in Figure 4.1. Each operator is characterized by its upper and lower switching fields. If the magnetic field becomes greater than the upper switching field or less than the lower switching field, the element will assume a positive state or negative state, respectively. The element, however, retains its state when H is between the lower and upper switching fields. The magnetization of the element is M_S or $-M_S$ in the positive and negative state,

respectively. The total magnetization is equal to the summation of the magnetization of all elements.

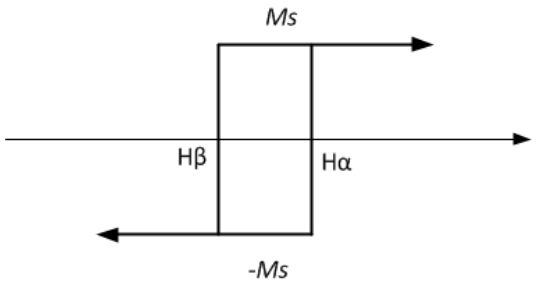

Figure 4.1. Hysteresis element of the Preisach model

In mathematical language the classical Preisach theory can be expressed by:

$$M(H) = \iint_{\alpha>\beta} \mu(\alpha,\beta)\gamma_{\alpha\beta}(H)d\alpha d\beta \tag{4.10}$$

,where $\mu\ (\alpha,\beta)$ is the distribution function or weight function and $\gamma\alpha\beta(H)$ describes the state of the hysteresis element (M_S or $-M_S$).

$$\gamma_{\alpha\beta} = \begin{cases} +M_S & H > H_\alpha \\ -M_S & H < H_\alpha \\ keep\ previous\ state & H_\beta < H < H_\alpha \end{cases} \tag{4.11}$$

, when it is assumed that:

$$-H_{\max} < H_\beta, H_\alpha < H_{\max} \tag{4.12}$$

,where H_{max} is the magnetic field density related to the maximum magnetization, M_{max}, in the major hysteresis loop.
The main advantage of the model is its accuracy in predicting the hysteresis trajectory even for minor loops and complex trajectories. However, practical implementation of the model for the finite element method and circuit simulation software involves serious difficulties that can be listed as follows:

1- The determination of the distribution function needs a large amount of experimental data.
2- The numerical evaluation of the double integral requires a large amount of time and memory.

3- The determination of the state of each hysteresis element requires the use of a composite algorithm instead of a mathematical expression.
4- In the model the input is H and output M, while the inverse model is required.

Over the years researchers have tried to solve or present practical methods for overcoming these problems. The main approach to modifying the classic method has been based on the "Everett" function [37] [49]. This method uses a graphical approach to the Preisach model, and converts the double integration into a summation of several Everett functions. In fact, the Everett function is a weighted integration in the triangular region of the Preisach diagram.
Determination of this function needs several first-order reversal curves. Several researchers have worked on determining the Everett function, together with the development of algorithms in order to implement this method [37]. However, because of the need for experimental data that are not easy to obtain, the absence of a direct mathematical function and obstacles to inverting the model, there still exists no "ideal" model as mentioned earlier.

4.2 Differential approach of scalar hysteresis

For modeling static scalar hysteresis a novel differential approach based on the classical Preisach theory is developed in this work. The model can predict hysteresis as accurate as the classic Preisach model. Furthermore, it has significant benefits. It can be easily inverted and has a simple algorithm; also, the data required for the model can be restricted to a set of first-order reversal curves. Moreover, the required experimental data can be minimized still further by using methods for estimation of the first-order reversal curves.
The proposed approach is implemented in a reluctance network method that will be described in chapter 6. The model is described in details in Paper I.
The model can be summarized by the expression below:

$$\frac{dB}{dH} = f(H, H_r) \quad \forall\ dH \succ 0\ \&\ H \succ H_r \tag{4.13}$$

$$\frac{dB}{dH} = g(H, H_r) \quad \forall\ dH \prec 0\ \&\ H \prec H_r \tag{4.14}$$

, where H_r is the last reversal point, and the golden rule is that after closing a minor loop the two reversal points corresponding to that loop will be omitted from the list of reversal points. The functions f and g can be obtained by using a set of the first-order reversal curves as described in Paper I.
The inverse of the model can be easily derived as follows:

$$\frac{dH}{dB} = F(H, H_r) \quad \forall\ dH \succ 0\ \&\ H \succ H_r \tag{4.15}$$

$$\frac{dH}{dB} = G(H, H_r) \quad \forall\ dH \prec 0\ \&\ H \prec H_r \tag{4.16}$$

, where F and G are inverse functions of f and g, respectively.

4.2.1.1 Validation

If the first-order reversal curves are available from measurement data, it is preferable to use them. Otherwise the abovementioned method can be used. Thus, improvement of the methods for the prediction of FORC can enhance the model. In order to verify the performance and accuracy of the model, a comparison between the measured and calculated hysteresis trajectories has been done for some grain-oriented electrical steels. The measurement method is the one described in Chapter 3. Figure 4.2 compare the modelled and measured symmetric hysteresis loops. In these comparisons a set of measured first order reversal curves are used for modeling.

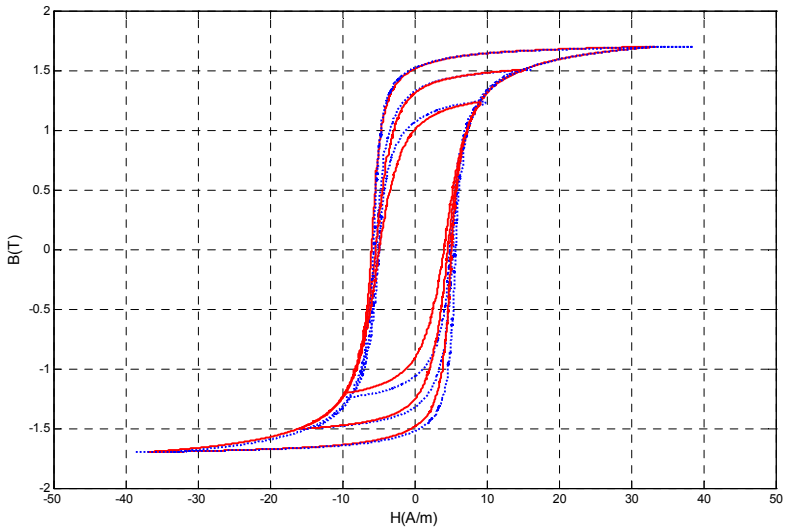

Figure 4.2. Comparison between measured and modelled hysteresis loops

(dashed lines are modelled and continuous lines are measured).

Chapter 5

5 Study on DC magnetization by FEM simulation

5.1 Finite element modeling

The finite element method (FEM) is a powerful tool for solving the electromagnetic equations [50] [51]. In recent decades, FEM has been widely used for modeling of transformers. The method is used to calculate core losses [52], magnetization current [53], stray losses [54] [55], leakage reactance [56], lumped model parameters [57] and electromagnetic forces [58].In contrast of its accuracy, the main restriction of it is its huge demand of computer time and memory. Hence, it is usually employed for research and validation purposes instead of the design process.

Transformers have a complex three dimensional geometry in general [21]. It is reasonable to simplify the model for certain purpose of modeling as much as possible. For the magnetic modeling of power transformers the insulation parts can be considered as air and only considering windings, core and metallic part would be important. Also, the complete model of the mentioned parts with details is not possible in practice and the model should be adapted according to expected purposes and requirements of the simulation.

The main goal of modeling in this stage of the project is realizing how the superimposed DC current that is consequence of an induced DC voltage can affect core saturation, magnetization current, core losses and stray-field profile in the transformer. It can help us to understand the phenomena and the difference between various transformer designs against it.

Therefore, this study needs a three dimensional, transient (time-dependent) analysis that includes core nonlinearity. The finite element domain should be connected to an external electrical circuit.

The program OPERA by Vector Fields [59] is employed for the modeling in this work, and all models are created by parametric scripts that allow changing the geometry and other parameters easily.
The study of DC magnetization with load condition is required to consider the reaction due to the network. However, there are some inherent and computational limitations in this task. For instance, connecting two transformers in two separate finite element models through electrical circuits is not possible in the current commercial software. Therefore, this finite element modeling is dedicated to no-load conditions and the transformer itself, and the aim is to understand the phenomena and use the result to build up and validate a nonlinear distributed reluctance network method that will be introduced in chapter 6. With that method the study of a transformer including interaction with the network becomes feasible.

5.1.1 Core model

As described in 2.3.2, the core is made of very thin laminations of electrical steels with overlapping in the joint regions. In practice, due to the huge amount of required elements, solving a finite element problem for such a geometry is infeasible. Fortunately, there are some facts that justify a simplification of the core model. The first is that at the frequency range of this study the skin depth of the core material is much greater than the thickness of the lamination. This means that the eddy currents don't affect the flux density distributions considerably. The second is that most of modern power transformers are made with steplap joints with a few steps. Our study shows that the performance of those joints would be good enough to approximate them as ideal joints. Therefore, the core geometry in the model consists of packets of limbs and yokes with ideal joints. For instance, the core model of a three phase three limb transformer is shown in Figure 5.1.

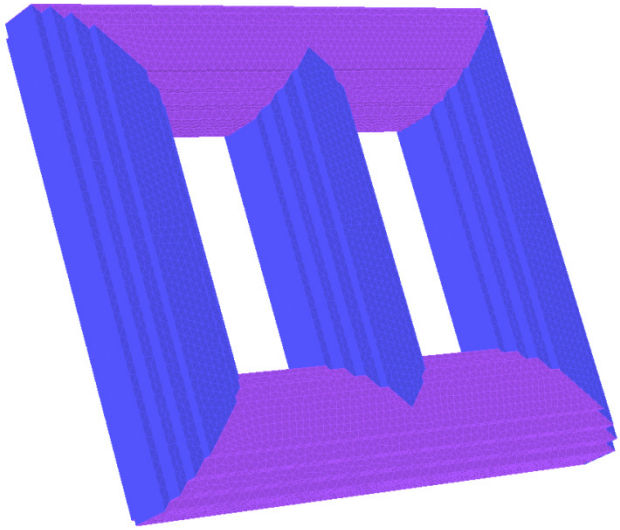

Figure 5.1. Core model of three phase three limb power transformer in the finite element method

For the core material the conductivity is set to zero, since the eddy current effects are ignored as mentioned before. The tensor of permeability is used for the core materials as:

$$\mu_r = \begin{bmatrix} \mu_{r,x} & 0 & 0 \\ 0 & \mu_{r,y} & 0 \\ 0 & 0 & \mu_{r,z} \end{bmatrix} \tag{5.1}$$

The relative permeability can be determined by a *B-H* curve that is different for each direction. It means that nonlinearity and anisotropy of the materials are taken into account. Because of limitations of the used software the hysteresis is neglected. However, the hysteresis losses are considered in the post-processing stages during the core loss calculation procedure.

5.1.2 Winding model

In practice, windings comprise multi-turn conductors. Each conductor, in turn, consists of parallel strands. The cross section area and the shape of strands are designed to avoid non-uniform current density distribution due to eddy current.

Nevertheless, according to the frequency range of this study one can assume that the current density has a uniform distribution on overall cross section of the winding. Therefore, the winding can be model as a cylindrical object with a uniform current density distribution in it.
Therefore, the conductivity and relative permeability of the winding material is set to zero and one, respectively. Nevertheless, the total resistance of winding, number of turns and filling factor should be determined.

5.1.3 Tank model

The tank geometry is considered to be an empty rectangular box. In this stage of simulation the material is assumed to have constant relative permeability equal to 1000 and no electrical conductivity. Taking into account the eddy currents inside the tank demands a drastic increase of the number of elements, which could lead to a very heavy computational load.

5.1.4 Symmetry

Due to symmetry the computational load can be reduced to one eighth and one fourth of the geometry of single phase and three phase transformers respectively. The symmetries are applied by setting proper normal and parallel boundary conditions [51]. Figure 5.2- Figure 5.5 show the models of various types of transformers with applied symmetry. The cross-sectional area of the core, and height of core window and windings, are the same for all types of transformers that are modelled in this study. This allows better comparison between different designs.

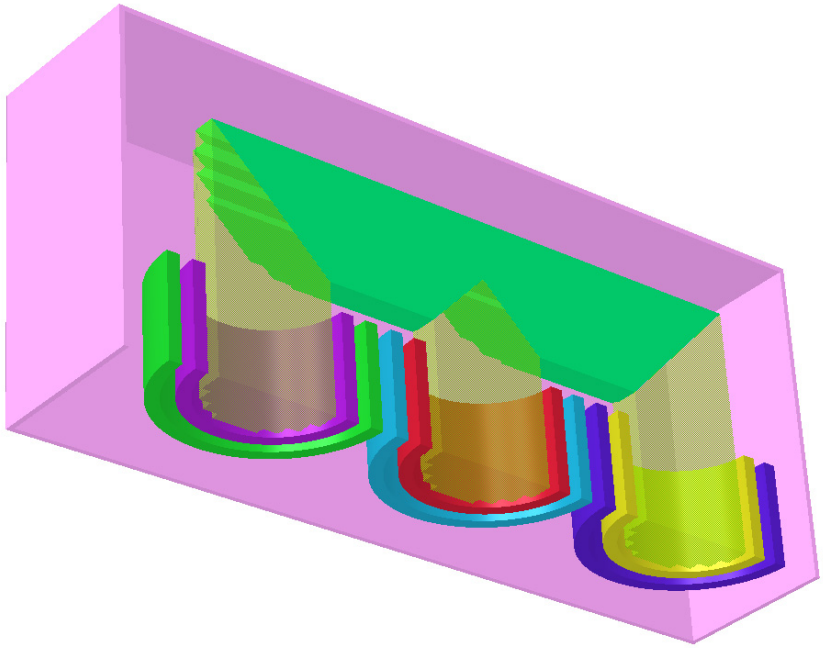

Figure 5.2. Three phase three limb transformer model with 1/4 symmetry.

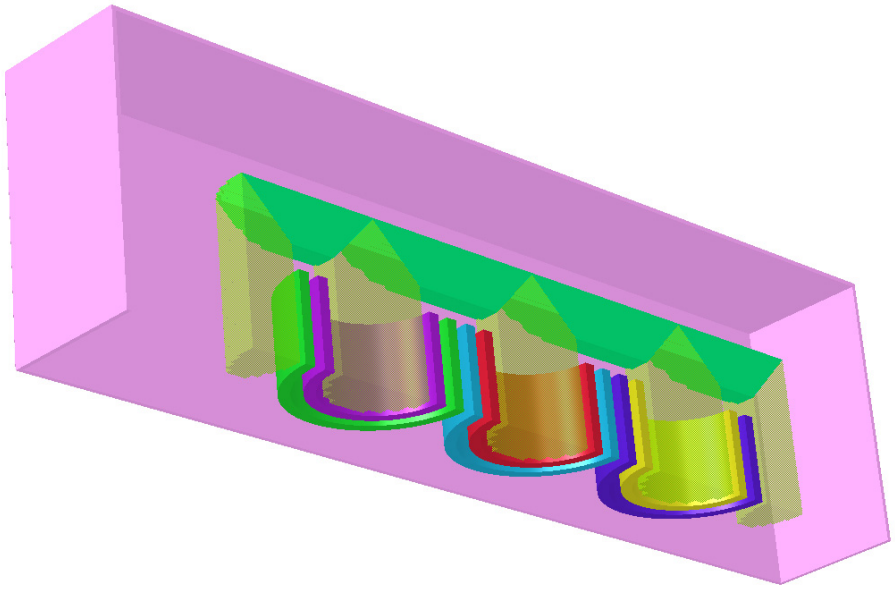

Figure 5.3. Three phase five limb transformer model with 1/4 symmetry.

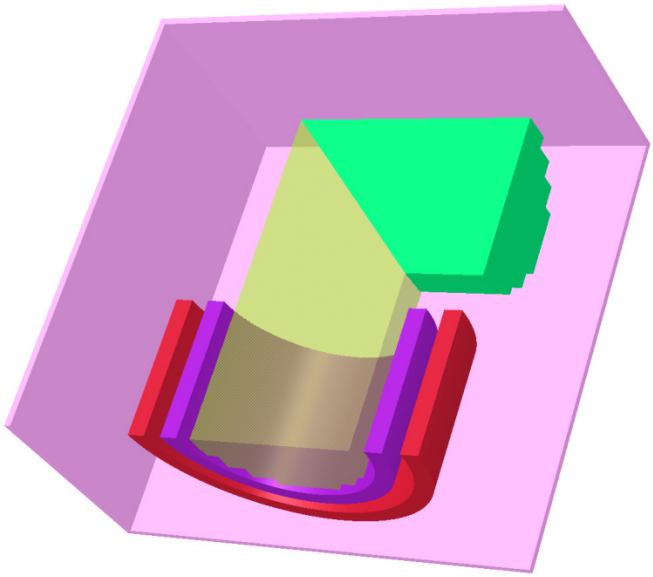

Figure 5.4. Single phase two limb transformer model with 1/8 symmetry.

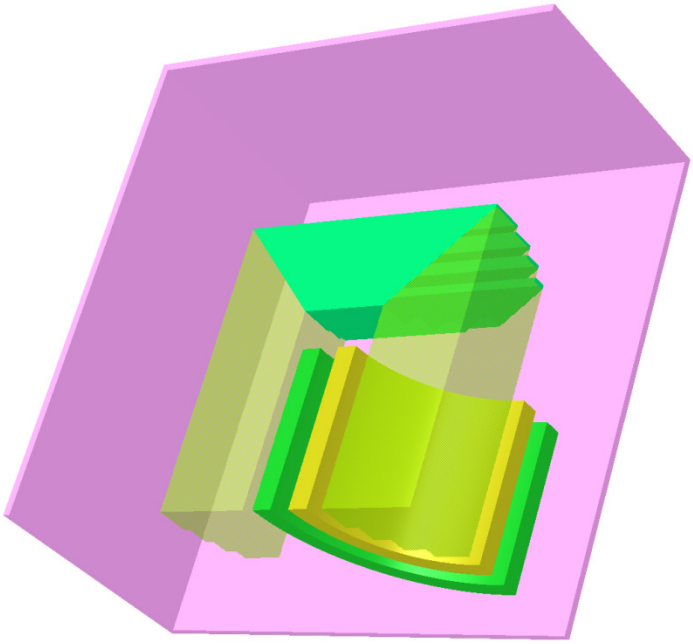

Figure 5.5.Single phase three limb transformer model with 1/8 symmetry.

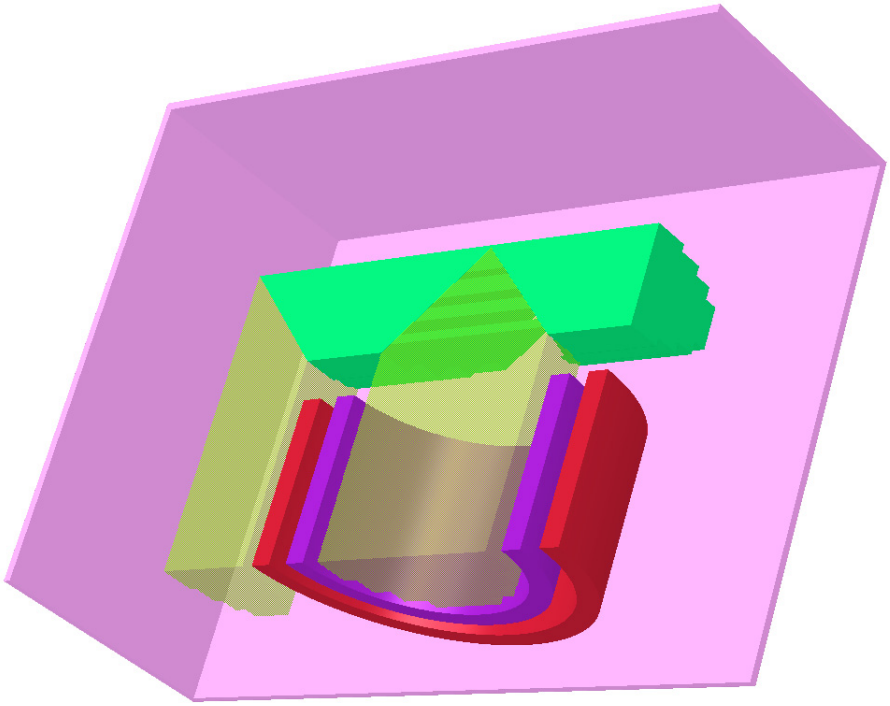

Figure 5.6. Single phase four limb transformer with 1/8 symmetry.

5.1.5 Circuit coupling

The connections of single phase and three phase transformers to external circuits are sketched in Figure 5.7 and Figure 5.8, respectively.
It is assumed that the injected DC current is the same in each phase of a three phase transformer or bank of single phases. This is because the DC resistance determines the distribution of the DC current and we assume that it is the same for the path of DC current for each phase, consisting of transformers and transmission lines. Therefore, to study the effect of DC current on no-load conditions of power transformers the high voltage winding of each phase is connected to the DC current source and a resistor in series. The LV windings are connected to the voltage source. For three phase transformers the connection type of the LV winding is a delta connection that is usual for step up transformers in power plants.

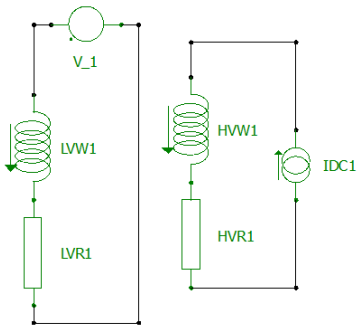

Figure 5.7. External circuit coupled with single phase transformers.

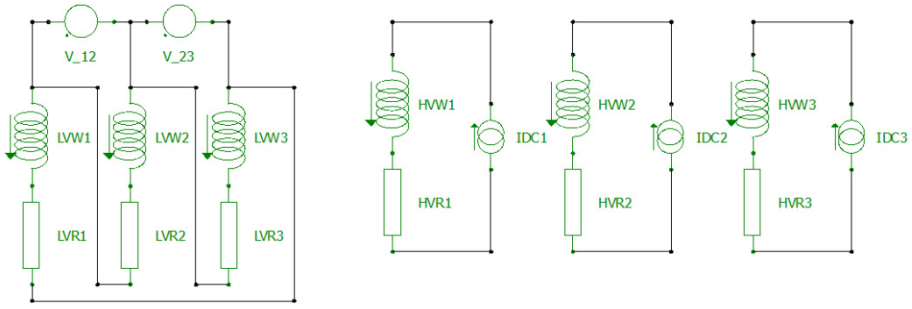

Figure 5.8. External circuit coupled with three phase transformers.

5.1.6 Soft start energization

There is a transient phenomenon during the energization of RL circuits with an AC voltage [60]. This transient, which is damped through the resistance of the circuit, typically takes several cycles to decay in transformer circuits. Therefore, in time-dependent finite element analyses it wastes a lot of time and computational effort to reach the steady state condition that is in the field of interest. In this work a soft-start energization is developed for omission of this transient. The soft start process takes less than quarter of a cycle and after that the real voltages are applied. The idea of soft start energization is to increase or decrease currents, voltages and fluxes from zero until the linkage flux in each phase reaches the value of the flux in the steady state condition corresponding to the start point of the applied voltage. The applied voltages during soft start energization can be obtained by:

$$V_{start}(t) = \left(\frac{\beta V_{\max}}{2\pi f}\sqrt{1-\left(\frac{V_{start}}{V_{\max}}\right)^2} - 0.5\, t_s\, V_{start}\right)\frac{t}{T_{start}} \qquad (5.2)$$

, where V_{max}, V_{start} and f are maximum of the main sinusoidal voltage, the main voltage at the moment after the soft start and the frequency of the main voltage, respectively. T_{start} and t_s are the duration of the soft start period, and time step of the simulation, respectively. β can be set to +1 or −1 and determines the sign of the slop of V_{start}. β depends on phase of the main voltage at the moment when soft start finish and the main voltage is applied.

Figure 5.9 and Figure 5.10 show the magnetization currents of a three phase transformer with the soft start energization method and corresponding applied voltages, respectively.

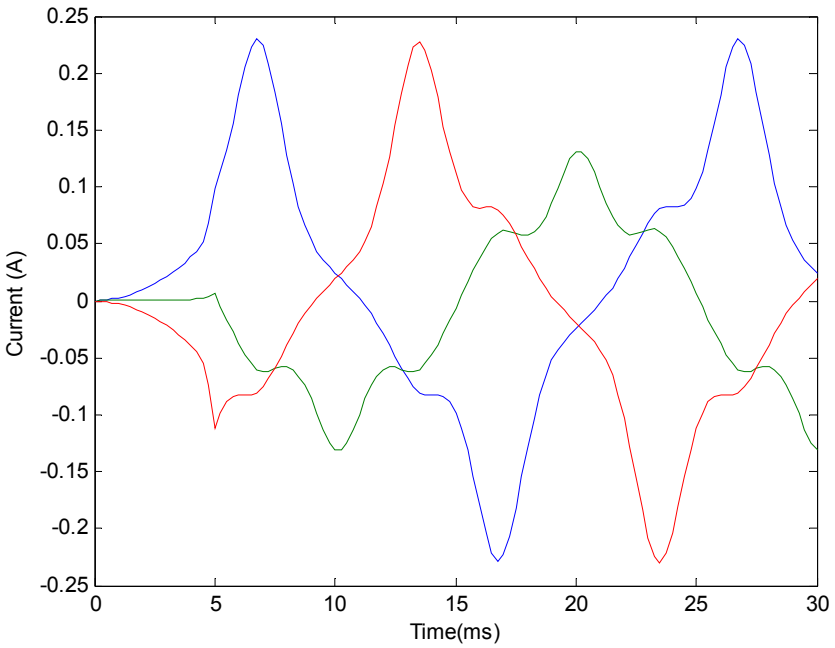

Figure 5.9. Magnetization currents of a three phase transformer with the soft energization.

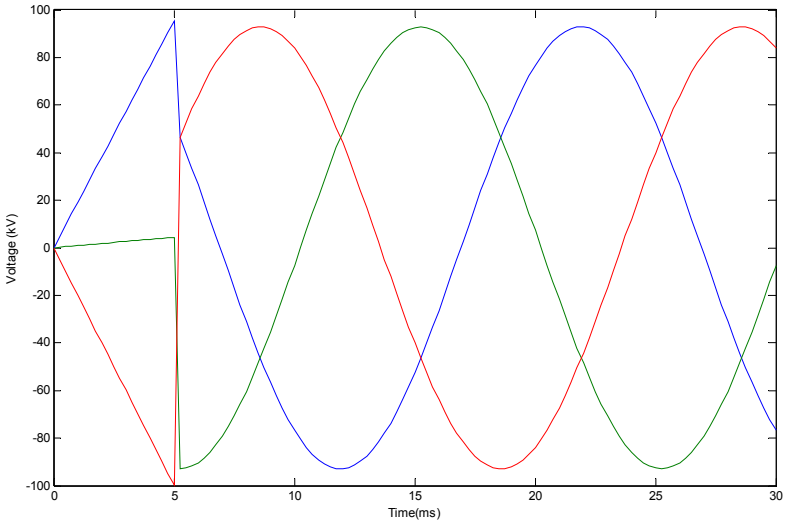

Figure 5.10. Applied voltages with soft energization.

5.2 What happens during a GICs attack

As mentioned before geomagnetically induced currents in transformers pass through the grounded neutral point of a star connection. The grounded neutral point creates the closed path that permits DC current through windings of transformers and transmission lines. The typical network for description of the phenomenon is illustrated in Figure 5.11.

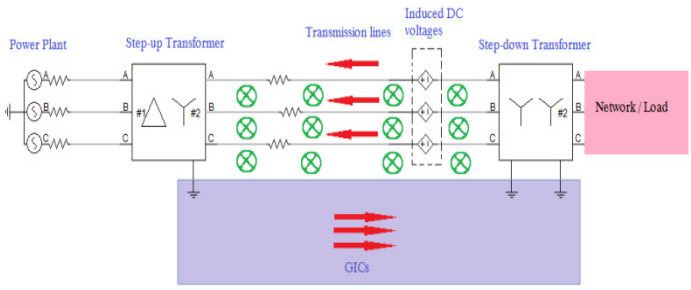

Figure 5.11. Typical network for description of GICs attack.

As explained in many papers [1]-[14] the DC current saturates the core of transformer within a half cycle and causes a non-symmetric magnetization current. The DC current leads to a DC offset in the linkage flux of the winding due to magnetization of the core. A famous diagram that is referred to in many studies in order to explain the phenomenon is shown in Figure 5.12.

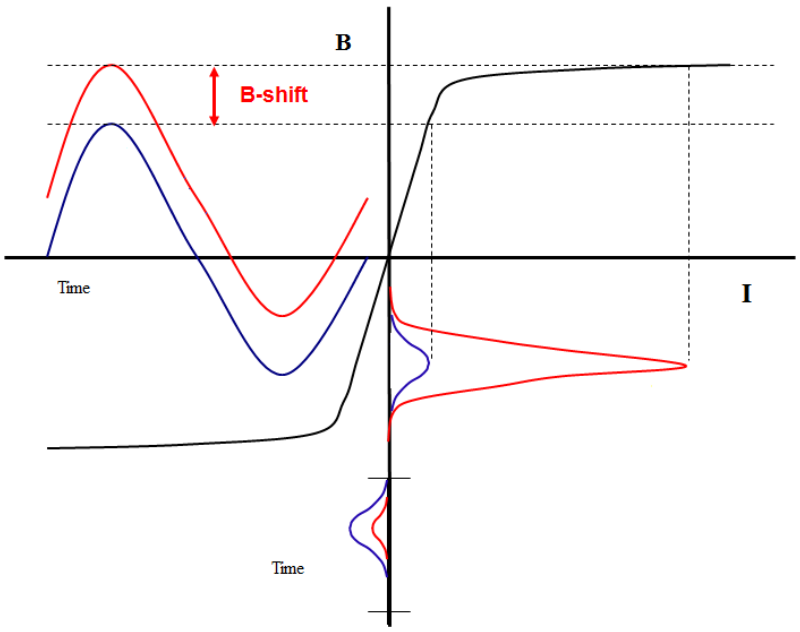

Figure 5.12. A very simple illustration of the effect of DC magnetization on the magnetization current.

However, what happens during GIC events is not as simple as mentioned above. In fact, the network deals with a quasi-DC voltage source instead of the current source. As a result of the interaction between solar winds and the magnetic field of the earth a flux passes near the ground with a quasi-DC variation. When this flux passes through a closed loop of conductors it causes an induced quasi-DC voltage, according to Faraday's law. This loop can consist of ground, grounded star-connected windings of transformers, and transmission lines, as illustrated in Figure 5.11. Therefore, it is obvious that longer transmission lines create a bigger loop and trap more flux, leading to higher induced voltage. This voltage according the type and strength of the phenomenon can be between 1 and 100 V/km and can last for couple of minutes to a couple of hours.

Consider that the DC voltage drops across the two grounded points of the transformers that is shown in Figure 5.11. Because of that according to Faradays' law the linkage flux of each winding, λ, will increase as:

$$\Delta\lambda = \int (V_{DC} - RI(t))dt \tag{5.3}$$

, where V_{DC}, R and I are the induced DC voltage, total resistance of the loop and current flowing in the loop, respectively. To attain such a linkage flux in the winding a proper magnetomotive force (MMF) is required. It means that a current should flow through the winding in the loop. The amount of the required current depends on the corresponding magnetic circuit. It is clear from (5.3) that if there is no resistance in the loop, the flux will keep increasing. Nevertheless, there is some resistance consisting of the transmission lines, windings and earths. Therefore, the increase of the flux continues until the corresponding current reaches the level where the total resistive voltage drop in the loop becomes equal to induced DC voltage. In that moment, a DC current flow in the circuit that is known as a geomagnetically induced current, GIC. Therefore, one can say that the amount of GIC is determined by the induced DC voltage and the total resistance in the loop.

In the beginning the induced flux passes almost entirely through the core. So, the required MMF would be low. However, if the flux continues increasing, the core will go to the saturation region, which means the MMF should increase drastically. But it is not the end of scenario. The core material cannot magnetize more than up to a certain limit. After that the core functions similar to air. Therefore, much higher MMF is required to cause a given level of flux, such that a much higher current must flow in the windings. One example of simulation results for a single phase transformer that shows this described transient is shown in Figure 5.13.

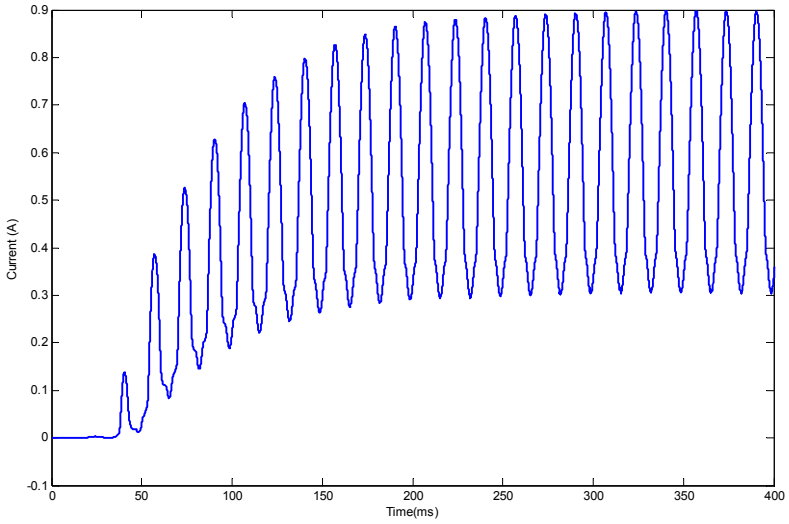

Figure 5.13. Transient phenomenon to stabilize GIC.

Since the high voltage windings have high number of turns, even small DC currents can be enough to saturate the core. Consider the step up transformer on the left side of Figure 5.11. What happens in low voltage side? The low voltage windings are connected to the power generators that create three phase AC voltage with 50 Hz or 60 Hz. Again, Faraday's law of induction says that the linkage flux in each low voltage winding should changes with the same frequency of voltage and proportional to the maximum of the voltage.
Consider that the direction of flux due to the GIC is in the positive direction i.e. above zero. Let's start at the moment when the phase voltage becomes negative. The linkage flux of the low voltage winding then should decrease. Without GIC in the steady state normal condition, the linkage fluxes change between the up and down knee points of the core saturation curve. This means that the returning points of the linkage flux are located on the knee points as shown in Figure 5.12. However, with existence of GIC the turning point in the positive direction occurs at a higher level. As a result the magnetization current should start to going down from a high current point. From another point of view, one can say that the magnetic circuit is in saturation and its behaviour is similar to that in air. Therefore, a small change of the flux demands a great change of the current. The decrease of the flux and the magnetization current continues and gets the core back to the non-saturated region. Since during saturation condition, the change of the flux then cannot be very much. At the moment then the voltage becomes positive, the flux should increase again.

What is the value of the magnetization current at this returning point? At that point the core is in the non-saturated region. Thus, the current of the low voltage winding should compensate the effect of the GIC to bring the core out of saturation. This means that the minimum absolute value of this returning point depends on the GIC level and usually is near to absolute value of it. This minimum value can also depend on the core and winding structure that will be discussed later in this section.
The difference between the maximum and the minimum of the magnetization current can reach the nominal load current and even more. The magnetization current increases and decreases drastically after the positive knee point. The duration of this is about 2-5 msec. As a result, the magnetization current becomes very non symmetric as shown in Figure 5.14 and contains higher harmonics.

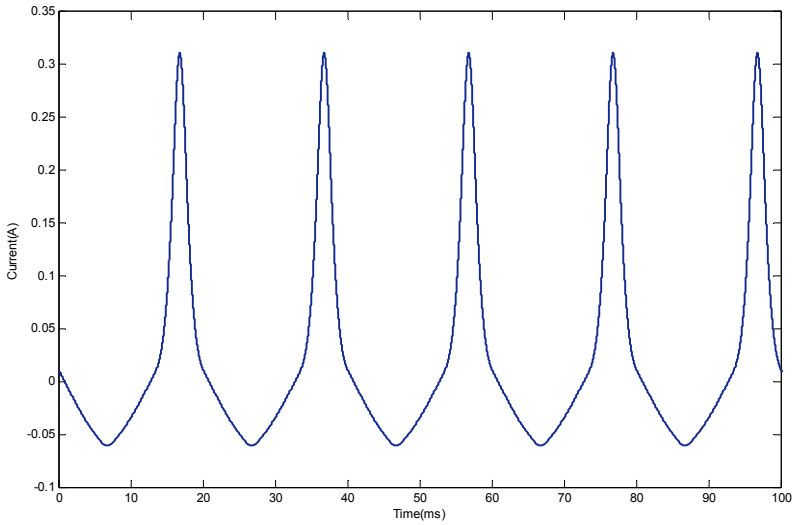

Figure 5.14. Magnetization current of a single phase transformer due to a low GIC level.

The other interesting issue is the peak value of the magnetization current. At first it seems to depend on the GIC current and of course the amplitude and phase of the applied voltage. However our study shows that the peak value of the magnetization current at steady state condition in the presence of GIC cannot exceed a certain value. Here, the meaning of "steady state condition" is the state that lasts for minutes to hours during a GIC attack. Therefore, higher GIC levels do not lead to higher magnetization current under steady sate condition. The reason is that at first there is a transient state lasting for few seconds and during this the peak value of the magnetization current decays to reach a steady state value. The maximum steady state value is equal to the

smallest magnetization current caused by GIC that completely can saturate the core. This can in other word be formulated as that in the worst case a GIC driven stationary DC offset of the core magnetization occurs around the knee point. The reason for this is the resistances of generators, transmission lines and transformer windings. When the magnetization current gets a high value the resistive voltage drop increases corresponding and results in an inductive voltage decrease across the transformer winding. It means that the required change of the flux in each half cycle decreases. Consequently, in each cycle the peak point of the magnetization current decreases a little and the upper returning point becomes closer to the knee point. This damping is faster at the beginning since the current and the corresponding resistive voltage drop are greater. The turning point then moves closer to the knee point such that the current becomes smaller and so the resistive voltage drop. Thus, the damping decreases and eventually becomes negligible. After that the described steady state begins. It is obvious that the damping is intensified by increasing the resistance. One example of a simulation result of this transient for a single phase transformer is shown in Figure 5.15.

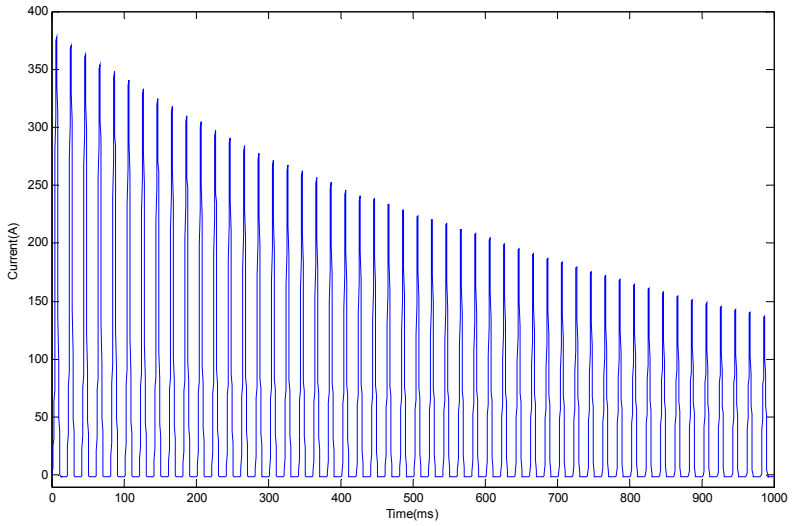

Figure 5.15. Transient of non-symmetric magnetization current due to GIC to reach steady state condition.

The described mechanisms of two types of transients that can occur due to geomagnetic phenomena are shown for a simple case in Figure 5.13 and Figure 5.15. In practice, these mechanisms can occur simultaneously and depend on network and transformer parameters.

The simulation results demonstrate that single phase transformers are sensitive to GICs. The various core types, comprising two limb, three limb and four limb, show similar behaviour. The reason is that the DC current easily can saturate the core in single phase transformers. In contrast, a three phase three limb transformer is very resistant against GIC. This is because of the structure of the core. DC currents compensate the effect of each other's in the main limbs and connecting yokes. As a result the core doesn't saturate easily and consequently it is not so affected by GIC. Nevertheless, three-phase five limb transformers behave more similarly to single phase transformers. Although DC currents compensate their effects of each other in the main limbs and their connecting yokes, they enhance each other to saturate the return limbs. That's way their behaviour is similar to single phase ones. Figure 5.16-Figure 5.20 show the magnetic flux density distribution in various core types of single and three phase power transformers due to a GIC current with a value around the maximum magnetization current without GIC. Figure 5.21 also shows the magnetic flux distribution of a three phase three limb power transformer for a GIC near to one hundred times of the maximum magnetization current under normal condition.

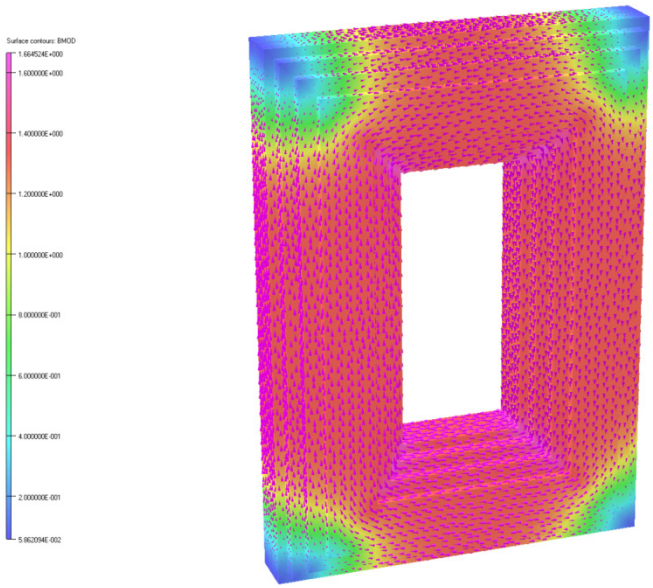

Figure 5.16. Flux distribution due to GIC in the core of a single phase two limb power transformer.

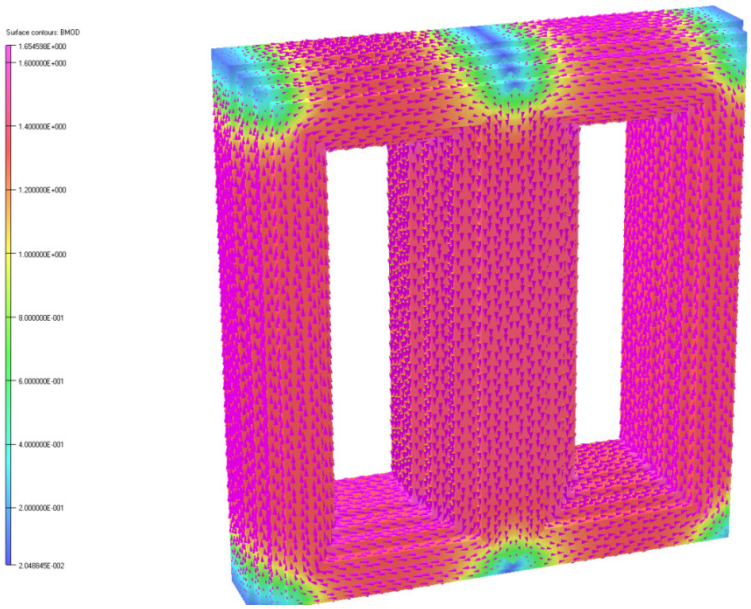

Figure 5.17. Flux distribution due to GIC in the core of a single phase three limb power transformer.

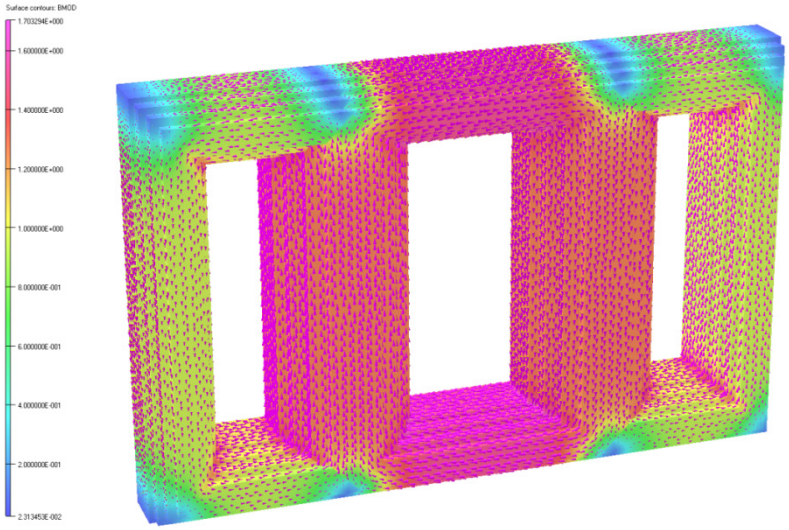

Figure 5.18. Flux distribution due to GIC in the core of a single phase four limb power transformer.

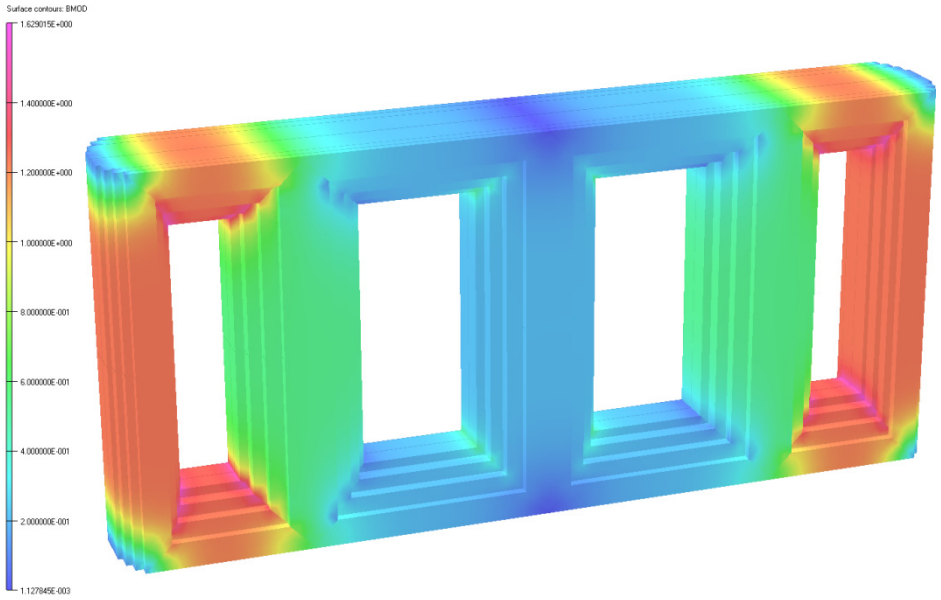

Figure 5.19. Flux distribution due to GIC in the core of a three phase five limb power transformer.

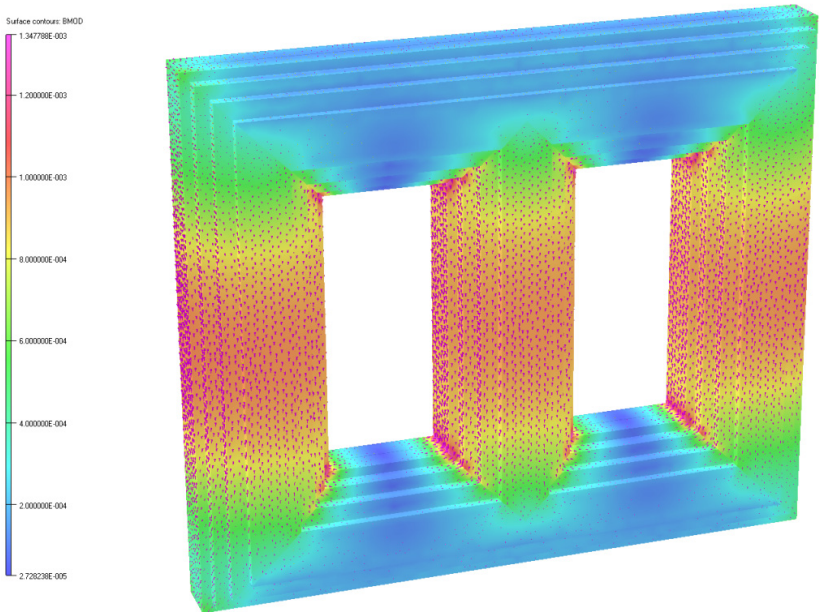

Figure 5.20. Flux distribution due to GIC in the core of a three phase three limb power transformer.

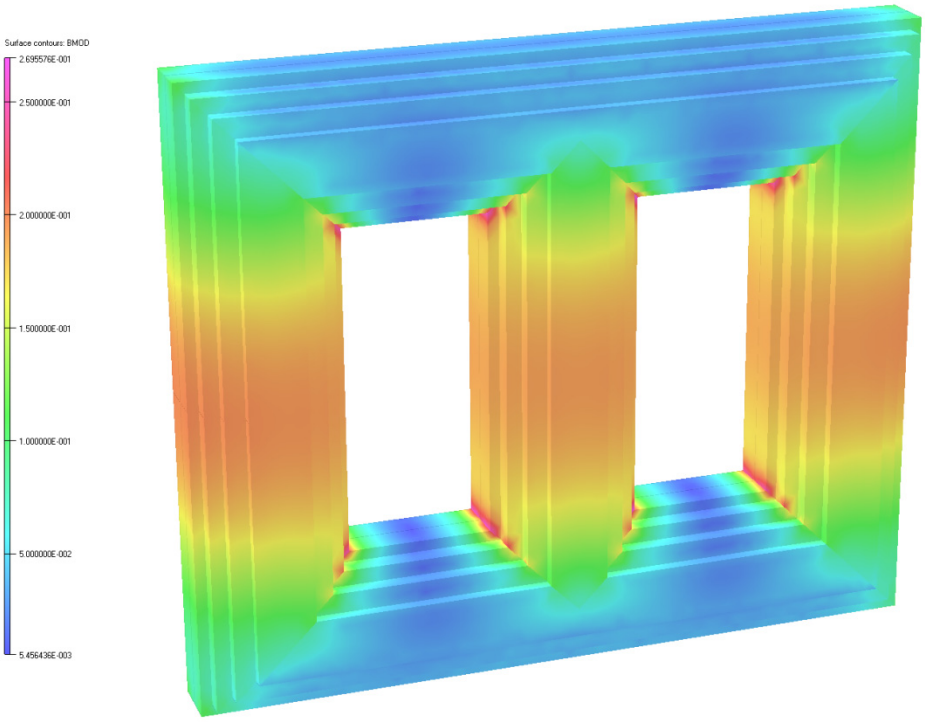

Figure 5.21. Flux distribution due to high value GIC in the core of a three phase three limb power transformer.

Therefore, it can be concluded that the three phase three limb transformer has best performance against GIC, as is demonstrated in our study and other researches [61]. However, it should be noticed that this is from the view point of the network. If one look at transformer itself this conclusion might not be valid during all conditions. Consider the left side transformer in Figure 5.11. When GICs pass through the high voltage windings the minimum value of the magnetization ampere-turn in the low voltage winding is near to the GIC's ampere-turn in the other side current. On the other word, there is an offset of DC current in the order of the referred GIC on the other winding. This is true except for a three phase three limb core with a minimum value in the same order as the normal magnetization current. This becomes significant when the stray fields and corresponding losses are important. In other types of core the GIC effect on the stray field can be compensated by the mentioned DC offset and only the difference between maximum and minimum magnetization current plays a role. The duration of the effect is short. However, in a three phase three limb core, the effect of GICs on stray fields is not compensated and the duration of the effect is whole power cycle. As a result, in the case of high level GIC attacks, the losses, hot spots and electromagnetic forces due to

stray fields could be noticeable and dangerous for the transformer. Also, if there is any unbalance condition that causes non-uniform distribution of GICs between the phases, the core saturates easily and harmful effects will appear.
So far, it is realized that during the GICs attacks, apart from the steady state condition that has been paid attention to in researches up to now, transient phenomena occur that also can be important both from the viewpoints of the transformers themselves and protection of the power network. Some simple simulations with saturable transformers in PSCAD prove that the transient and steady state condition can be affected by changes of the combinations of transformers on both sides of a transmission line. For instance, the combination of a bank of transformers with a three phase three limb transformer shows different behaviour than two banks of single phase transformers. The simulated model in PSCAD is shown in Figure 5.22. However, the currently available transformer models in circuit simulation programs are not accurate enough to obtain reliable results regarding investigation of GICs. For example they are not good enough to consider air paths that are important during a GIC attack.

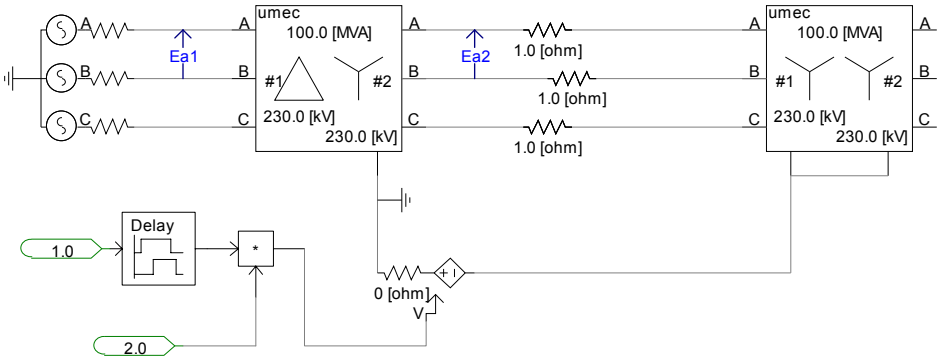

Figure 5.22. Transformer and network model in PSCAD for simulation of the effects of GICs.

Therefore, a comprehensive study of the phenomenon needs an appropriate electromagnetic model of power transformers coupled with circuit analysis program. The demand of computational time and memory for this task is not possible to fulfil with the finite element method, in practice. However, this method is anyway used in this work for qualitative understanding of the phenomenon and to verify the nonlinear distributed reluctance network method that is introduced in Chapter 6. Comprehensive analysis of the transient phenomena and effect of the load, combinations of transformers and other network parameters will be done by using a reluctance network method in the next phase of this work aiming of a PhD degree.

5.3 Effect of GIC on core losses

5.3.1 Calculation method

The losses in the core material depend on the waveform of flux density. The flux density waveform is different in different regions of the core. Hence, the feasible approach for accurate core-loss calculation can be divided in three stages. The first is finding the magnetic flux density waveform in each element of the core. The next is the calculation of losses for each element. Eventually, by integration of losses throughout of whole core volume, the total losses can be obtained.
The flux density waveforms are found by use of finite element simulations. Calculation of the resulting losses requires consideration of the physics of the losses.
The method for calculation of losses for arbitrary flux density waveforms based on Bertotti's loss separation theory is described in Paper II by the author of this thesis. Also in that paper a method for estimation of static hysteresis loops with the DC offset that appears during a GIC attack is suggested.

5.3.2 Results and discussion

The results regarding the increase of core losses due to GICs for single phase transformers are presented by the author in detail in Paper II. The results show that the core losses can increase up to 50% in steady state condition when the DC offset of the average flux density is about 0.6 T. The point is that such a DC offset occurs even for small GICs. On the other hand higher GICs also lead to such DC offsets under steady state condition as described before. The other thing is that different core types for single phase transformers have a similar behaviour for the same DC offset of the average flux density. However, four limb cores and three limb cores need higher DC currents to reach the same DC offset of the average flux density, compared to two limb cores. In three phase power transformers, a five limb core has similar behaviour as single phase transformers and the core losses can under steady state condition increase up to 60%. Again the three phase three limb transformer constitutes an exception. The increase of core losses even for high GICs is moderate. Another point regarding core losses is that for transformers that are designed for a lower average flux density under normal conditions, the percentage of core losses increase more due to GICs.

5.4 Effect of GIC on the Magnetization Current

Saturation of a transformer core in one of the half cycles causes a very non symmetric magnetization current which contains both odd and even harmonics. These higher harmonics increase winding and stray losses in the metallic parts of the transformer. Furthermore, they can be important for the network and protection relays. In this section the created harmonics due to GICs in steady state condition are investigated for various core types. The simulations have been performed for all mentioned types of power transformer. The step up transformer on the left side of Figure 5.11 was the example used in the simulations. The magnetization current has been obtained for several levels of GICs and applied voltages. The Fast Fourier Transform (FFT) has been employed for finding the frequency spectrum of the magnetization current waveforms.

5.4.1 Single phase transforms

Single phase power transformers show similar behaviour regarding the magnetization current. For instance, the magnetization currents for the single phase two limb transformer without GIC, with GIC current near 50% of maximum normal magnetization current, and with GIC near to maximum normal magnetization current are shown in Figure 5.23- Figure 5.25. Also, Figure 5.26- Figure 5.28 demonstrate the corresponding frequency spectrums. The amplitude of each harmonic is normalized to the peak value of the time-domain current waveform.

Analysis of the results shows that under normal magnetization current, first, third and fifth harmonics are dominant. However, in the presence of GIC second and fourth harmonics are enhanced. And, as was expected, the waveform contains a considerable DC component as well. The amplitude of the main harmonic can reach 30-40 % of the maximum magnetization current, which can reach nominal load current and even more. It means that the winding at least should endure 30-40% overload.

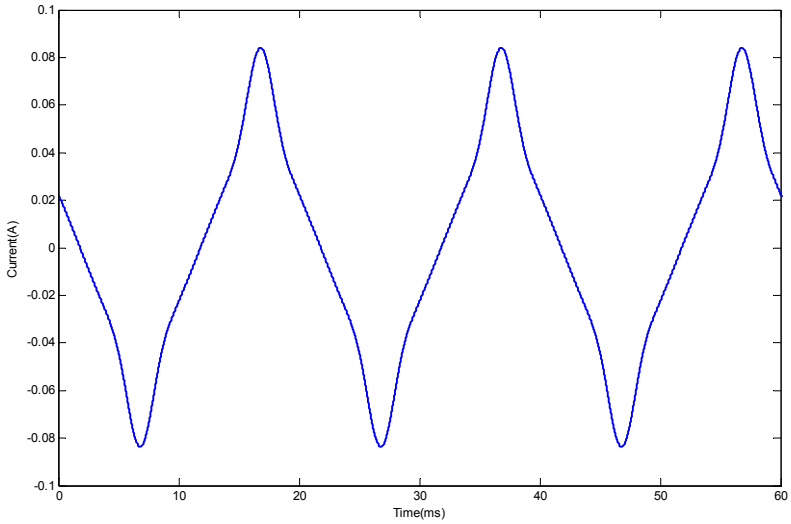

Figure 5.23. Magnetization current of a single phase two limb transformer without GIC.

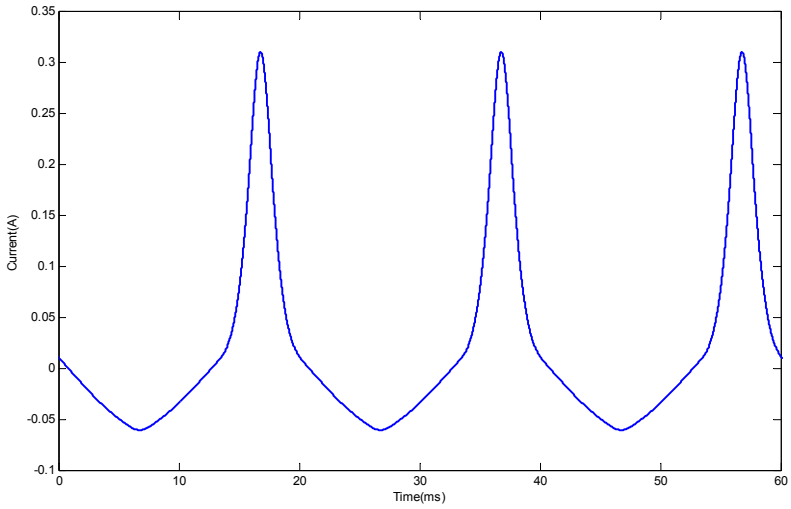

Figure 5.24. Magnetization current of a single phase two limb transformer with GIC near 50% of maximum normal magnetization current.

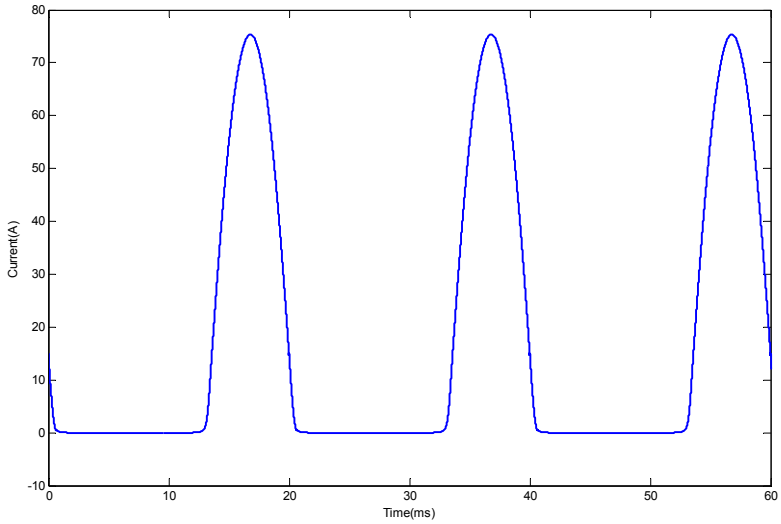

Figure 5.25. Magnetization current of a single phase two limb transformer with GIC near 100% of maximum normal magnetization current.

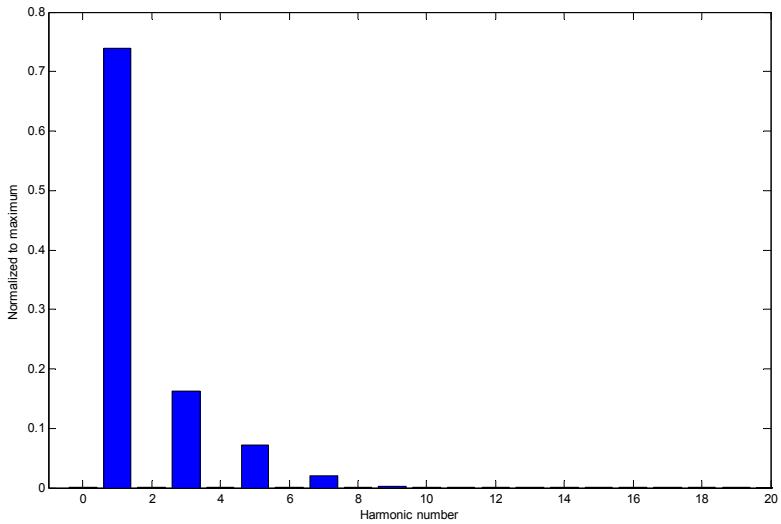

Figure 5.26. Spectrum of a single phase two limb transformer without GIC.

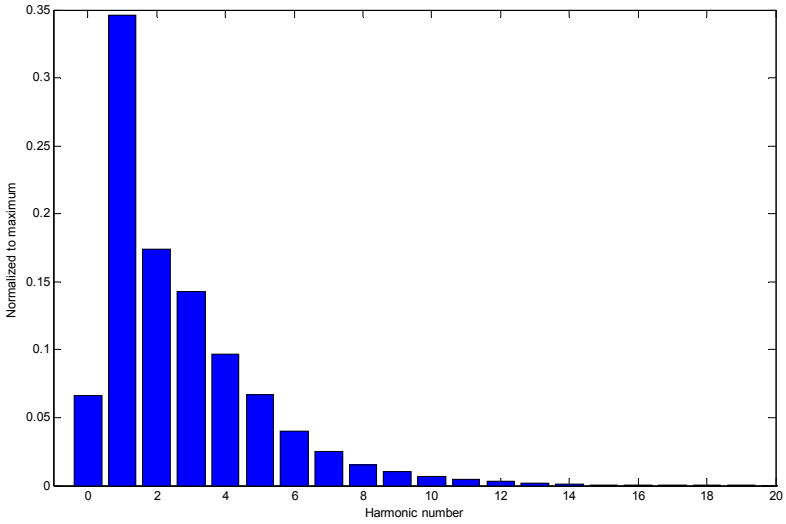

Figure 5.27. Spectrum current of a single phase two limb transformer with GIC near 50% of maximum normal magnetization current.

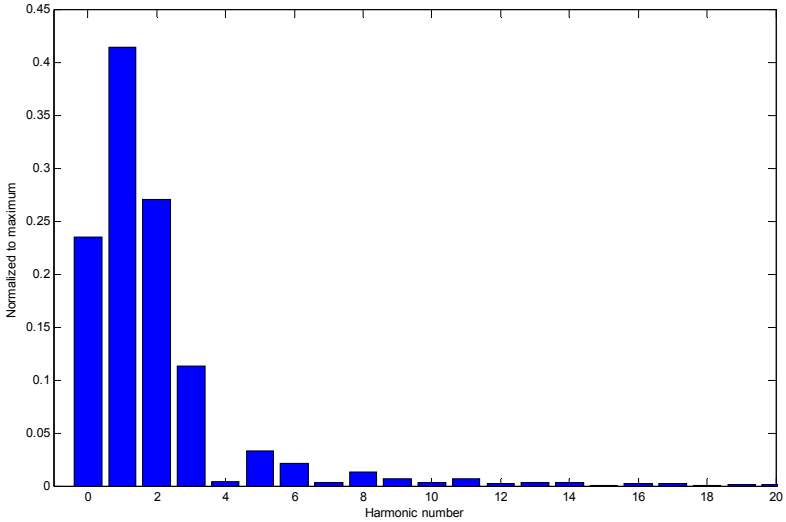

Figure 5.28. Spectrum current of a single phase two limbs transformer with GIC near 100% of maximum normal magnetization current.

5.4.2 Three phase transformers

As it was expected the behaviour of three phase three limb transformers is different from three phase five limb transformers. Though five limb transformers function similar to single phase ones regarding GIC, the magnetization current shows a small difference.
The magnetization currents and spectrum of one of the phases under normal condition without GIC for a three limb transformer is shown in Figure 5.29 and Figure 5.30, respectively. The magnetization current of this type of transformers do not show considerable change for low GIC levels. Figure 5.31 and Figure 5.32 show the magnetization currents and frequency spectrum in the case of a high GIC level that is near 100 times maximum normal magnetization, respectively. It is obvious that GICs has not a significant impact on the amplitude of the magnetization current. Although the even harmonics increase, they still are relatively small.

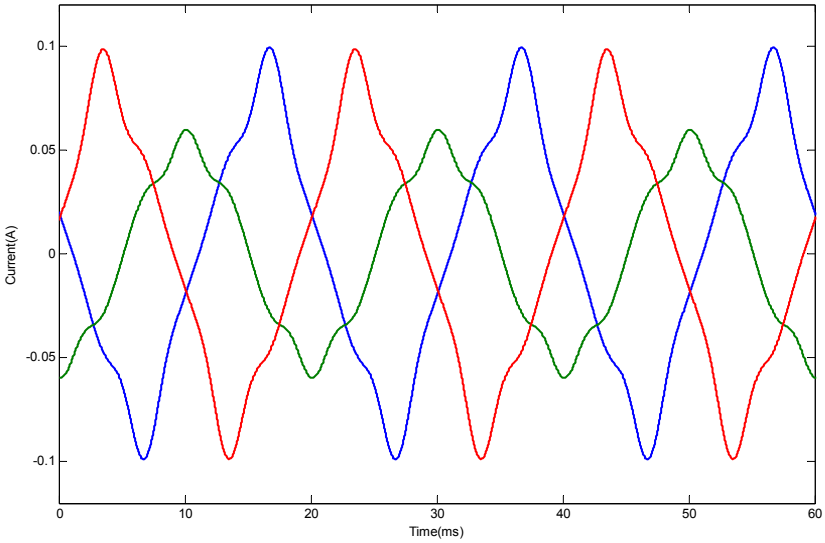

Figure 5.29. Magnetization currents of three phase three limb transformer without GIC.

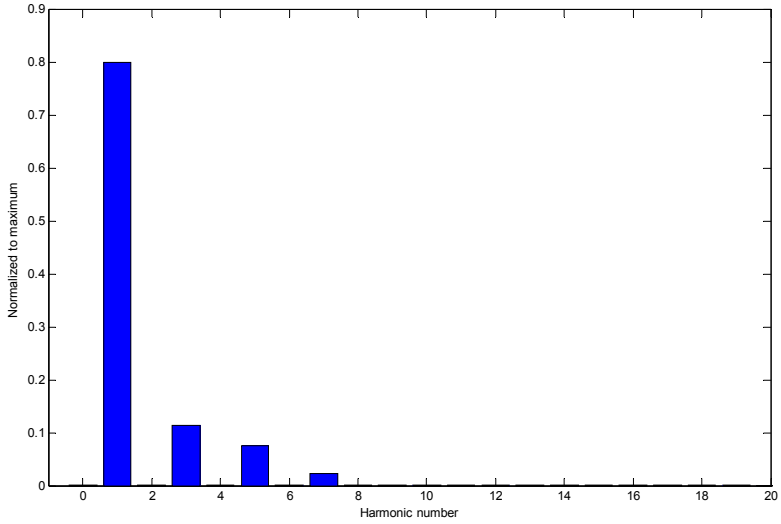

Figure 5.30. Spectrum of a three phase three limb transformer without GIC.

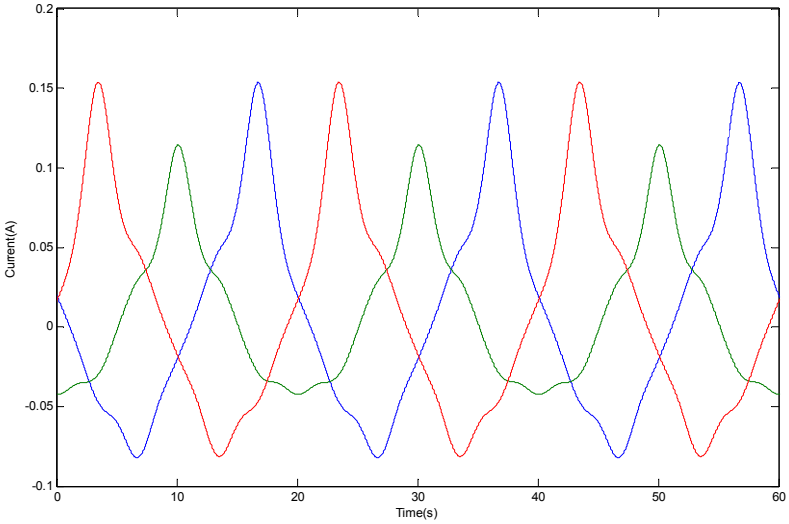

Figure 5.31. Magnetization currents of a three phase three limbs transformer with a high GIC level.

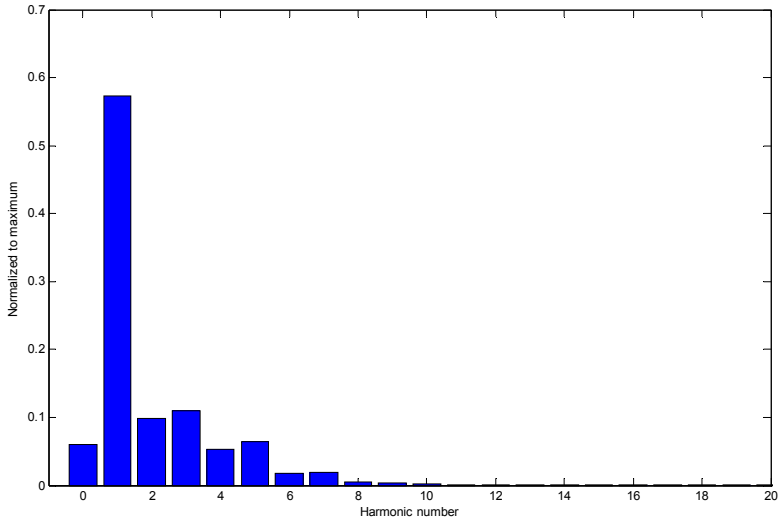

Figure 5.32. Spectrum of a three phase three limb transformer with a high GIC level.

Magnetization currents of a five limb transformer and the corresponding frequency spectrum are illustrated in Figure 5.33-Figure 5.34, respectively. Comparison with Figure 5.29 reveals that unlike the three limb transformer the magnetization currents in each phase of the five limb transformer have the same magnitude. Figure 5.35 and Figure 5.36 show the magnetization currents and frequency spectrum with GIC near half of the maximum normal magnetization. It shows that the GIC can affect the magnetization current of a five limb transformer such as a single phase one but more intensely. Also, the fifth and four harmonics are larger than the third one. They also are different from the current waveforms of single phase transformers such that the frequency spectrums after the main harmonic are descending.

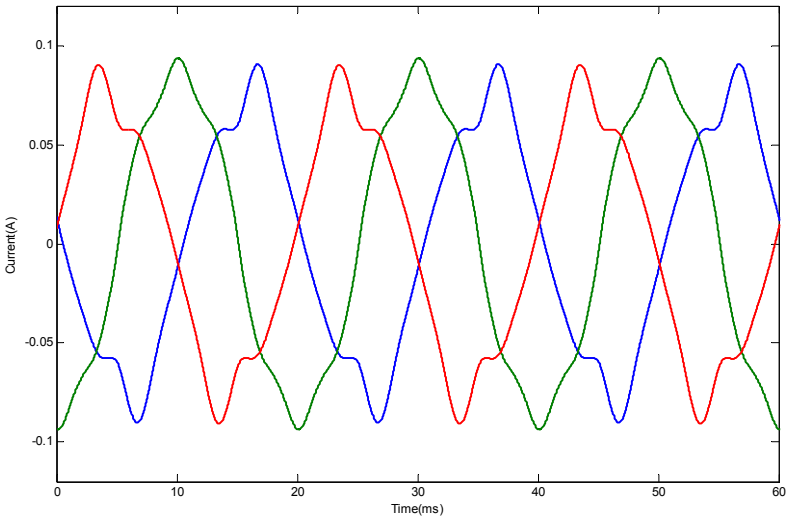

Figure 5.33. Magnetization currents of a three phase five limb transformer without GIC.

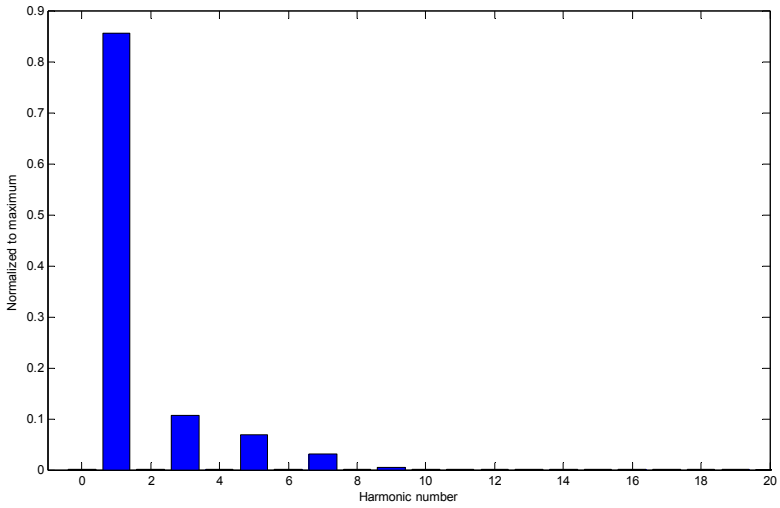

Figure 5.34. Spectrum of a three phase five limb transformer without GIC.

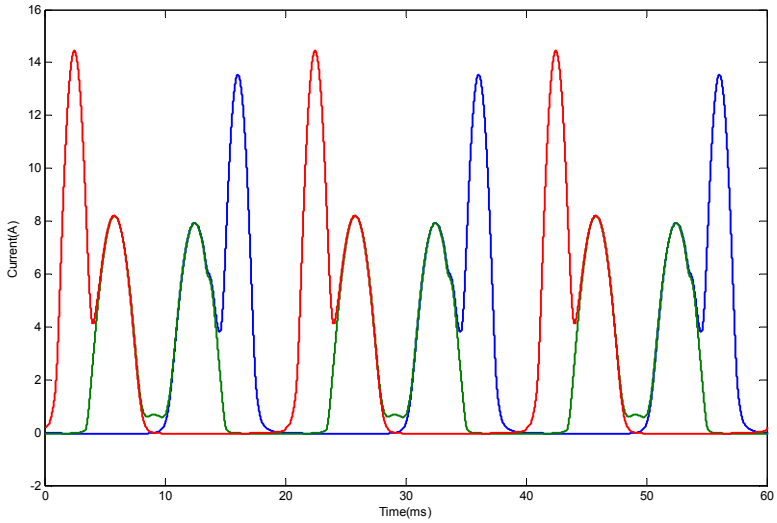

Figure 5.35. Magnetization currents of a three phase five limb transformer with GIC near 50% of maximum normal magnetization current.

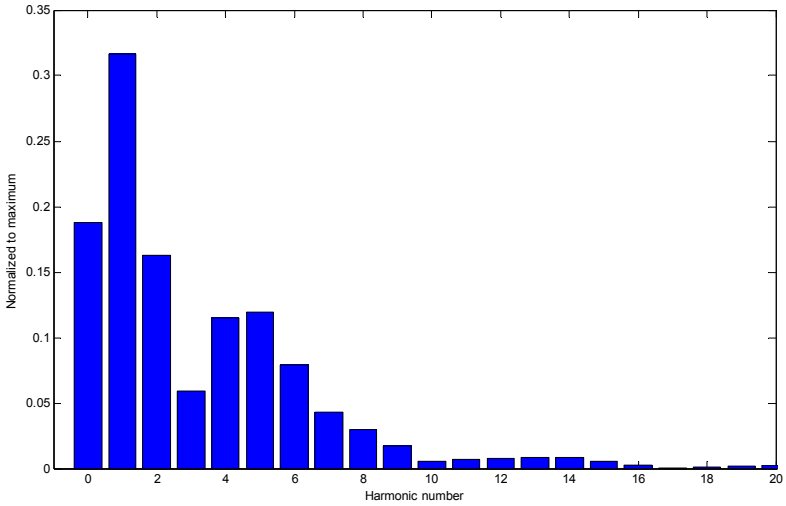

Figure 5.36. Spectrum of a three phase five limb transformer with GIC near 50% of maximum normal magnetization current.

Chapter6

6 Distributed Nonlinear Reluctance Network Model Approach

6.1 Introduction

The electromagnetic modeling of power transformers are widely used for the analysis of transients that occur regarding interaction transformers and the power grid. Also it is used for the parameter calculation that is needed for design purposes. The accuracy and complexity of the model depends on the aims that are expected to be achieved. The frequency range of the study is an important factor that determines level of details of the model that should be developed. Classification of transient phenomena and corresponding frequency ranges are proposed in [60]

- 5Hz to 1 KHz: slow transients.
- Power frequency up to 10 kHz: switching transients.
- 10 kHz up to 1MHz: fast transients.
- 100 kHz to 50 MHz: very fast transients.

The scope of this study regarding DC magnetization of power transformers is in the range of slow transients. In this frequency range an accurate model of transformer should take into account the core properly [26]. Since the core play the main role regarding low frequency transients. Also, the model should have the capability to couple with external electrical circuits that influence transient phenomena of the transformer.
As mentioned before, although the finite element method is very powerful in solving electromagnetic problem, it demands a lot of CPU time and memory that restricts its use in practice. It usually employed for understanding of phenomena and validation of other calculation methods. Since in this work the

field distribution inside the transformer is intended to be investigated, the low frequency models that are suggested in [14] [25] [26] cannot function. The aim of those models is to find the transient currents and voltages and also the parameters of the models must be found by use of other modeling techniques or measurements. Thus, a distributed reluctance network method (DRNM) can be a good alternative to FEM in electromagnetic problems with satisfactory computational speed and acceptable accuracy [62]. The applications of RNM in modeling of transformers have been described in [62] [63]. In [62] the distributed reluctance network method is presented and employed for calculation of stray fields and associated losses in power transformers. However, in that model the core model is linear and the reluctance network does not have any connection with external electrical circuits.

Therefore, to fulfil the aims of this study a distributed nonlinear reluctance network should be developed. A hysteresis model should be implemented in the model. Also, it should have the capability to be connected to electrical surrounding circuitry.

Developing such a model comprises the following tasks:

- Find a solution method for a nonlinear reluctance network connected to an external circuit for transient (time dependence) analysis.
- Find a proper method to take into account losses in the reluctances.
- Develop a method to create a reluctance network from a given geometry of transformer.

In this thesis the solution method for a nonlinear reluctance network with implementation of the hysteresis model has been done. This method is introduced in Paper III. The complementation of the model with the mentioned steps will be done in the continuation of this project leading to a PhD degree.

Chapter7

7 Future works

7.1 Finalize the already introduced hysteresis models

There are some hysteresis models that are introduced at KTH before the start of this PhD project. These are, however, waiting to be verified and developed further. The measurement system that has been developed in this project makes it possible to develop those further models.

7.2 Distributed Nonlinear Reluctance Network Model of Power Transformers

Tools for comprehensive electromagnetic modeling of power transformer of low and medium frequencies demand a method that can consider nonlinearity and hysteresis properties of core material and a three dimensional construction of transformers. Also, they should be capable to couple with external circuits for analysis of transients that occur due to interaction of transformer and the network. The goal in this project is to improve and extend the reluctance network method to a distributed nonlinear reluctance network such that the mentioned aspects can be covered. The method of solving the nonlinear network is developed in the first phase of the project. It will be continued by the development of a method that considers winding and stray losses and also an automatic creation of the distributed network by using the geometry of the transformer.

7.3 Protection and stability aspect

The GICs have adverse effects on both power transformer and the surrounding network. The asymmetric magnetization current due to GICs injects harmonics to network and it could lead to misoperation of protective relays. Hence, this part of the project will be dedicated to investigation of the issues that GICs create regarding protection aspects of transformer and network and suggest methods to improve the protection system. Finally, after understanding how the GICs affect power transformer and network, it is expected that the project comes up with suggestions for design of power transformer and settings of the protection in order to diminish the adverse effects of GICs.

7.4 Transformer model for using in power system simulation software

Nowadays, there are several well-known and widely used software for analysis of transient and steady-state conditions of power networks. PSCAD, EMTP are examples of such software. The suggestion of more accurate and comprehensive models of power transformers would be very valuable in power system studies.

7.5 Verifications of models and results

The developed models should be verified with experimental tests to be reliable for use in industry and future works. A proper design of a the test setup to make the intended experiments feasible is required.

Bibliography

[1] P. Price, “Geomagnetically induced current effects on transformers,” *Power Delivery, IEEE Transactions on,* vol. 17, no. 4, pp. 1002-1008, 2002.

[2] H. C. Tay and G. W. Swift, “ON THE PROBLEM OF TRANSFORMER OVERHEATING DUE TO GEOMAGNETICALLY INDUCED CURRENTS,” *IEEE Transaction on Power Apparatus and Systems,* Vols. PAS-104, no. 1, pp. 212-219, January 1985.

[3] I. T. a. D. Committee, “Geomagnetic disturbance effects on power systems,” *Power Delivery, IEEE Transactions on,* vol. 8, no. 3, pp. 1206-1216, 1993.

[4] R. Pirjola, “Geomagnetically induced currents during magnetic storms,” *Plasma Science, IEEE Transactions on,* vol. 28, no. 6, pp. 1867-1873, 2000.

[5] X. Li, X. Wen, P. Markham and Y. Liu, “Analysis of Nonlinear Characteristics for a Three-Phase, Five-Limb Transformer Under DC Bias,” *Power Delivery, IEEE Transactions on,* vol. 25, no. 4, pp. 2504-2510, 2010.

[6] C. Mao, S. Wang, J. Lu, G. Mei and D. Wang, “Measures of restraining DC current through transformer neutral point: A comprehensive survey,” in *Universities Power Engineering Conference, 2007. UPEC 2007. 42nd International*, 2007.

[7] B. Zhang, L. Liu, Y. Liu, M. McVey and R. Gardner, “Effect of geomagnetically induced current on the loss of transformer tank,” *Electric Power Applications, IET,* vol. 4, no. 5, pp. 373-379, 2010.

[8] R. Girgis and C.-D. Ko, “Calculation techniques and results of effects of GIC currents as applied to large power transformers,” *Power Delivery, IEEE Transactions on,* vol. 7, no. 2, pp. 699-705, 1992.

[9] C. Gaunt and G. Coetzee, “Transformer failures in regions incorrectly considered to have low GIC-risk,” in *Power Tech* , Lausanne, 2007.

[10] X. Dong, Y. Liu and J. Kappenman, “Comparative analysis of exciting current harmonics and reactive power consumption from GIC saturated transformers,” in *Power Engineering Society Winter Meeting, 2001.*

IEEE, 2001.

[11] S. Lu, Y. Liu and J. De La Ree, "Harmonics generated from a DC biased transformer," *Power Delivery, IEEE Transactions on,* vol. 8, no. 2, pp. 725-731, 1993.

[12] R. Walling and A. Khan, "Characteristics of transformer exciting-current during geomagnetic disturbances," *Power Delivery, IEEE Transactions on,* vol. 6, no. 4, pp. 1707-1714, 1991.

[13] B. Bozoki, S. Chano, L. Dvorak, W. Feero, G. Fenner, E. Guro, C. Henville, J. Ingleson, S. Mazumdar, P. McLaren, K. Mustaphi, F. Phillips, R. Rebbapragada and G. Rockefeller, "The effects of GIC on protective relaying," *Power Delivery, IEEE Transactions on,* vol. 11, no. 2, pp. 725-739, 1996.

[14] W. Chandrasena, P. McLaren, U. Annakkage and R. Jayasinghe, "An improved low-frequency transformer model for use in GIC studies," *Power Delivery, IEEE Transactions on,* vol. 19, no. 2, pp. 643-651, 2004.

[15] "IEEE standard test code for liquid-immersed distribution, power, and regulating transformers,".

[16] S. Kulkarni and S. Khaparde, Transformer Engineering: Design and Practice, New York. Basel: Marcel Dekke,r Inc., 2004.

[17] M. Heathcote, J & P Transformer Book, Thirteenth Edition, Elsevier Ltd., 2007.

[18] "IEEE Guide for Transformer Loss Measurement, C57.123-2010".

[19] I. Dasgupta, Design of Transformers, New Delhi: Tata McGraw-Hill, 2005.

[20] R. M. D. Vecchio and B. Poulin, Transformer Design Principles: With Applications to Core-Form Power Transformers, Second Edition, CRC Press, 2010.

[21] S. V. Kulkarni and K. S. A, Transformer Engineering: Design, Technology, and Diagnostics, CRC Press, 2012.

[22] F. Fiorillo, Measurement and Characterization of Magnetic Materials, Elsevier, 2004.

[23] F. Fiorillo, "Measurements of magnetic materials," *Metrologia,* vol. 47, pp. S114-S142, 2010.

[24] B. D. Cullity and C. D. Graham, Introduction to magnetic materials, IEEE Press, 2009.

[25] J. Martinez and B. A. Mork, "Transformer modeling for low- and mid-frequency transients - a review," *Power Delivery, IEEE Transactions on,* vol. 23, no. 3, pp. 1696- 1697, 2005.

[26] F. de Leon and A. Semlyen, "Complete transformer model for electromagnetic transients," *Power Delivery, IEEE Transactions on,* vol. 9, no. 1, pp. 231-239, 1994.

[27] Z. S., M. P., M. T. and M. A. J., "Use of novel adaptive digital feedback for magnetic measurements under controlled magnetizing conditions," *IEEE Transactions on Magnetics,* vol. 41, no. 11, pp. 4242-4249, 2005.

[28] Z. PÓLIK and M. KUCZMANN, "Measuring and control the hysteresis loop by using analog and digital integrators," *Journal of Optoelectronics and Advanced Materials ,* vol. 10, no. 7, pp. 1861-1865, 2008.

[29] Z. Polik, T. Ludvig and M. Kuczmann, "Measuring of the Scalar Hysteresis Characteristic with a Controlled Flux Density using Analog and Digital Integrators," *Journal of ELECTRICAL ENGINEERING,* vol. 58, no. 4, pp. 236-239, 2007.

[30] "IEC 404-2, Methods of measurement of the magnetic properties of electrical steel sheet and strip by means of an Epstein frame.," 1996.

[31] "IEC 404-3, Methods of measurement of the magnetic properties of magnetic sheet and strip by means of a single sheet tester," 1992.

[32] J. Sievert, "The measurement of magnetic properties of electrical sheet steel- survey on methods and situation of standards," *Journal of Magnetism and Magnetic Materials,* pp. 647-651, 2006.

[33] V. K. Madisett, Digital Signal Processing Fundamentals, CRC Press, 2010.

[34] D. C. Jiles and D. L. Atherton, "Theory of ferromagnetic hysteresis," *Journal of Applied Physics,* vol. 55, no. 6, pp. 2115- 2120, 84.

[35] A. Bergqvist, On Magnetic Hysteresis Modeling, Stockholm: Royal Institute of Technology, 1994.

[36] D. Ribbenfjärd, Electromagnetic transformer modelling including the ferromagnetic core, Stockholm: Royal Institute of Technology, 2010.

[37] I. D. Mayergoyz, Mathematical Models of Hysteresis, New York: Academic Press, 1990.

[38] F. Liorzou, B. Phelps and D. Atherton, "Macroscopic models of magnetization," *Magnetics, IEEE Transactions on ,* vol. 36, no. 2, pp. 418-428, 2000.

[39] G. Bertotti, Hysteresis in magnetism, San Diego: Academic Press, 1998.

[40] S. Cao, B. Wang, R. Yan, W. Huang and Q. Yang, "Optimization of hysteresis parameters for the Jiles-Atherton model using a genetic algorithm," *Applied Superconductivity, IEEE Transactions on ,* vol. 14, no. 2, pp. 1157-1160, 2004.

[41] P. Wilson, J. Ross and A. Brown, "Optimizing the Jiles-Atherton model of hysteresis by a genetic algorithm," *Magnetics, IEEE Transactions on ,* vol. 38, no. 9, pp. 989-993, 2001.

[42] A. Bergqvist, "A simple vector generalization of the Jiles-Atherton model of hysteresis," *Magnetics, IEEE Transactions on ,* vol. 32, no. 5, pp. 4213- 4215 , 1996.

[43] N. Sadowski, N. Batistela, J. Bastos and M. Lajoie-Mazenc, "An inverse Jiles-Atherton model to take into account hysteresis in time-stepping finite-element calculations," *Magnetics, IEEE Transactions on ,* vol. 37, no. 2, pp. 797-800, 2002.

[44] M. Mathekga, R. McMahon and A. Knight, "Application of the Fixed Point Method for Solution in Time Stepping Finite Element Analysis Using the Inverse Vector Jiles-Atherton Model," *Magnetics, IEEE Transactions on ,* vol. 47, no. 10, pp. 3048-3051, 2011.

[45] S.-T. Liu, S.-R. Huang and H.-W. Chen, "Using TACS Functions Within EMTP to Set Up Current-Transformer Model Based on the Jiles–Atherton Theory of Ferromagnetic Hysteresis," *Power Delivery, IEEE Transactions on ,* vol. 22, no. 4, pp. 2222-2227, 2007.

[46] D. Jiles, "A self consistent generalized model for the calculation of minor loop excursions in the theory of hysteresis," *Magnetics, IEEE Transactions on ,* vol. 28, no. 5, pp. 2602-2604, 1992.

[47] X. Wang, D. Thomas, M. Sumner, J. Paul and S. Cabral, "Characteristics of Jiles–Atherton Model Parameters and Their Application to Transformer Inrush Current Simulation," *Magnetics, IEEE Transactions on ,* vol. 44, no. 3, pp. 340-345, 2008.

[48] Z. Preisach, "Über die magnetische Nachwirkung. Zeitschrift für Physik," *Zeit. Phys.,* vol. 94, pp. 277-302, 1935.

[49] T. Doong and I. Mayergoyz, "On numerical implementation of hysteresis models," *Magnetics, IEEE Transactions on ,* vol. 21, no. 5, pp. 1853-1855, 2005.

[50] G. Meunier, The Finite Element Method for Electromagnetic Modeling, Wily, 2008.

[51] J. P. Av. Bastos and S. N., Electromagnetic Modeling by Finite Element Methods, NewYork. Basel: Marcel. Dekker, Inc., 2003.

[52] G. Loizos, T. Kefalas, A. Kladas and A. Souflaris, "Flux Distribution Analysis in Three-Phase Si-Fe Wound Transformer Cores," *Magnetics, IEEE Transactions on ,* vol. 46, no. 2, pp. 594-597, 2010.

[53] O. Biro, G. Buchgraber, G. Leber and K. Preis, "Prediction of Magnetizing Current Wave-Forms in a Three-Phase Power Transformer

Under DC Bias," *Magnetics, IEEE Transactions on ,* vol. 44, no. 6, pp. 1554-1557, 2008.

[54] D. Pavlik, D. Johnson and R. Girgis, "Calculation and reduction of stray and eddy losses in core-form transformers using a highly accurate finite element modelling technique," *Power Delivery, IEEE Transactions on ,* vol. 8, no. 1, pp. 239-245, 1993.

[55] X. M. Lopez-Fernandez, P. Penabad-Duran and J. Turowski, "Three-Dimensional Methodology for the Overheating Hazard Assessment on Transformer Covers," *Industry Applications, IEEE Transactions on ,* vol. 48, no. 5, pp. 1549-1555, 2012.

[56] S. Jamali, M. Ardebili and K. Abbaszadeh, "Calculation of short circuit reactance and electromagnetic forces in three phase transformer by finite element method," in *ICEMS*, 2005.

[57] E. Bjerkan, High Frequency Modeling of Power Transformers, Trondheim: NTNU, 2005.

[58] J. Faiz, B. Ebrahimi and T. Noori, "Three- and Two-Dimensional Finite-Element Computation of Inrush Current and Short-Circuit Electromagnetic Forces on Windings of a Three-Phase Core-Type Power Transformer," *Magnetics, IEEE Transactions on ,* vol. 44, no. 5, pp. 590-597, 2008.

[59] OPERA-3D User Guid, England: Vectorfield limited, 2003.

[60] J. A. Martinez-Velasco, Power System Transients: Parameter Determination, Taylor & Francis, 2009.

[61] R. Girgis and K. Vedante, "Effects of GIC on power transformers and power systems," in *Transmission and Distribution Conference and Exposition (T&D), 2012 IEEE PES* , 2012.

[62] J. Turowski, M. Turowski and M. Kopec, "Method of three-dimensional network solution of leakage field of three-phase transformers," *Magnetics, IEEE Transactions on ,* vol. 26, no. 5, pp. 2911-2919, 1990.

[63] D. Koppikar, V. Kulkarni and J. Turowski, "Fast 3-dimensional interactive computation of stray field and losses in asymmetric transformers," *Generation, Transmission and Distribution, IEE Proceedings,* vol. 147, no. 4, pp. 197-201, 2000.